Air temperature partitioning of snow accumulation, erosion and melt: a regime shift occurring on top of Mt. Ortles (Eastern Italian Alps)

Tiziana Lazzarina Zendrini[1], Luca Carturan[1], Michael Lehning[2,3], Mathias Bavay[2], Federico Cazorzi[4], Paolo Gabrielli[5], Nander Wever[2] and Giancarlo Dalla Fontana[1]

[1]Department of Land, Environment, Agriculture and Forestry, University of Padua, Legnaro, Italy
[2]WSL Institute for Snow and Avalanche Research SLF, Davos, Switzerland
[3]CRYOS, School of Architecture, Civil and Environmental Engineering, EPFL, Lausanne, Switzerland
[4]Department of Agriculture and Environmental Sciences, University of Udine, Udine, Italy
[5]Italian Glaciological Committee c/o University of Turin, Turin, Italy

Correspondence to: Tiziana Lazzarina Zendrini (tizianalazzarina.zendrini@phd.unipd.it)

Abstract. Glacier mass balance measurements and models are key tools for understanding the glacier response to climate change and specific processes occurring at the glacier surface. Snow accumulation and wind-driven erosion are among the most difficult processes to measure and model in high-altitude alpine terrain and on glaciers, due to their high variability in space and time, and to the scarcity of in situ observations. In addition, snow accumulation and erosion are key processes in the formation and preservation of ice core archives located on high-altitude accumulation areas of mountain glaciers, yet their impact on these paleoclimatic archives is still unquantified. In this study we used a rare dataset of nivo-meteorological and mass balance observations collected between 2011 and 2015 at 3830 m a.s.l. on Mt. Ortles (Eastern Alps) to investigate snow accumulation and erosion processes in close proximity to an ice core drilling site located in the upper accumulation area of Alto dell'Ortles Glacier. We applied the physics-based snow cover model SNOWPACK, constrained by field data, to reproduce the local mass balance and to explicitly simulate snow erosion by wind. The model reproduced the observed seasonal and annual mass balance variability with good accuracy over the four-year study period. Results indicate that wind erosion was the dominant ablation process at the study site, removing 21% of the snowfall, whereas melt played a minor role removing only 3%. Erosion was most effective in winter, during or shortly after snowfall events, and its efficiency was controlled by air temperature, with dry snow being much more susceptible to erosion (91% of total erosion) than wetted snow (9% of total erosion). Sensitivity experiments to air temperature perturbations demonstrated that wind erosion provides a negative feedback to the mass balance, because increasing temperature accelerates snow metamorphism and makes the snow surface less erodible. However, a further 1°C warming would promote a transition from an erosion-dominated to a melt-dominated mass balance regime. Our findings emphasize the importance of accounting for wind erosion in projections of glacier mass balance on high-elevation wind exposed glacierized areas. They also highlight the relevance of snow erosion for the interpretation of ice core records, because long-term variations in snow erosion may have affected the formation of the seasonal paleoclimatic signal and its preservation.

1 Introduction

The local mass balance dynamics of alpine glaciers are characterised by high variability in time and space, resulting from the interaction between atmospheric processes and the local topography. In addition, the glacier mass balance is regulated by multiple feedback mechanisms. Powerful positive feedbacks are the glacier cooling effect (Carturan et al., 2013; Shaw et al., 2023, 2025), albedo (Klok and Oerlemans, 2004; Johnson and Rupper, 2020), and elevation (Schäfer et al., 2017). Negative feedback are represented by debris and avalanche accumulation (Benn and Evans, 2014; Capt et al., 2016), topographic shadowing (De Marco et. al, 2020), cloud cover (Zhao et al., 2023). These mechanisms add complexity in the glacier mass balance response to atmospheric changes. Despite good knowledge obtained for single processes, accounting for their interactions in glacier mass balance models or in paleoclimatic reconstructions from glacier recorded data (e.g. ice cores) is highly challenging, also because they lead to non-linearities in the climatic response of glacier systems (Ayala et al., 2015; Carrivick et al., 2015; Hock and Huss, 2021).

A main source of uncertainty affecting glacier mass balance models, or reconstructions from proxy data, concerns snow accumulation (Clark et al., 2011; Hock et al., 2017), which typically exhibits complex spatial patterns and high time variability, especially at high-elevation and wind-exposed areas. Wind action is indeed responsible for preferential snow deposition (Lehning et al., 2008), erosion and redistribution, which result in a spatial distribution of snow which is strongly dependent on wind speed, direction and interaction with the local topography (Clark et al., 2011; Mott et al., 2011, 2018).

High-elevation and wind-exposed ice caps and saddles in the accumulation areas of glaciers are often selected for ice core drilling, for paleoclimatic and paleoenvironmental reconstructions. These sites are suitable for ice core drilling for the dominant vertical and minimum horizontal flow of the snow/ice but also because of low air temperature, which preserves climatic and environmental proxy data from melt water percolation, and low snow accumulation rate (due to snow redistribution by wind), which enable recording paleoclimatic and paleoenvironmental data spanning periods of time from seasonal to multimillennial time scales in the Alps (Konrad et al., 2013; Gabrielli et al., 2016; Bohleber et al., 2019). However, dating and reconstructing paleoenvironmental conditions from ice and firn cores extracted at these sites may be biased, because wind can remove a large fraction of the total accumulated snow, potentially erasing precipitation that occurred over entire months or seasons (e.g. Lehning et al., 2008).

Proxy system models (models that describe the processes by which environmental conditions are recorded in a glacial archive) are often used to improve dating and reconstruction of past climatic conditions obtained from ice/firn cores (e.g. Evans et al., 2013). For instance, these models calculate how stable water isotopes are recorded in ice core archives, generating a pseudo proxy that is compared to the actual water isotopes, to constrain its paleoclimatic interpretation (typically air temperature). These models implicitly assume negligible year-to-year variation of snow redistribution, melt, and meltwater percolation, meaning that they do not explicitly calculate the glacier mass balance and do not take into account its variability over time.

Low latitude drilling sites are increasingly affected by atmospheric warming and loss of seasonal or even annual snow accumulation due to enhanced melt. Considering these conditions, Carturan et al. (2025) proposed a proxy system model that explicitly accounts for the glacier mass balance and melt variability over time. When compared to traditional annual layer counting of stable isotope and pollen seasonal oscillations for producing an ice core chronology, the authors found that the model significantly improved the interpretation of the firn stratigraphy during the 1996-2011 warm period at the high-altitude drilling site of Mt. Ortles, in the Eastern Alps. Among possible further improvement of their model, Carturan et al. (2025) mentioned the addition of a simple parameterization of snow erosion and its dependence on air temperature.

In this context, a critical simplification affecting most glacier mass balance models regards the calculation of snow accumulation and wind redistribution, and in particular their long-term response to variations in air temperature/wind intensity. Snow accumulation is generally handled statistically, using precipitation data recorded by automatic weather stations at lower elevation. Precipitations are extrapolated on glaciers using multiplication parameters that account for the vertical gradients of precipitation and its redistribution. These parameters are tuned using available observations of mass balance and/or remote sensing-derived snow cover (e.g. Schuler et al., 2005; Huss et al., 2008; Carturan et al., 2012; Cremona et al., 2025) and are assumed to be constant over time. This approach, normally used due to the scarcity of direct observations of snow redistribution, implicitly assumes that the relationship between low-elevation precipitation and snow accumulation on glaciers is fixed over time. However, as suggested by Haeberli and Alean (1985) and reported by Li and Pomeroy (1997a) and He and Ohara (2017), there is strong evidence that air temperature regulates the susceptibility of the snowpack to wind erosion. The wind speed threshold for initial motion is controlled by snow metamorphism that, along with other factors such as snow wetness, kinetic friction, and elasticity, is controlled by air temperature (Li & Pomeroy, 1997b).

As a result, the role of air temperature on snow susceptibility to wind erosion can be considered a potentially relevant negative feedback. Because cold and dry snow at high elevations is more easily eroded by wind than temperate snow (often containing refrozen melt layers), it is possible that the annual snow accumulation rate and/or the seasonal magnitude of snow erosion are changing significantly in response to atmospheric warming (Haeberli and Alean, 1985), but this process has not yet been quantified. In this case, paleoclimatic reconstruction from ice/firn cores would significantly benefit from improved modelling of the relationship between snow erosion and air temperature/wind conditions.

In this study, we investigated the snow processes observed at an automatic weather station operated between 2011 and 2015 at 3830 m a.s.l., next to the Mt. Ortles drilling site at 3859 m a.s.l., where detailed meteorological and snow observations are available (Carturan et al., 2023). Using the physics-based process-oriented SNOWPACK model (Lehning et al., 2002a, 2002b), which explicitly accounts for snow erosion by wind, we characterised the snow erosion process in close proximity to this drilling site, which can be considered as representative of high-elevation and wind-exposed areas of alpine glaciers were firn and ice cores are usually retrieved. We analysed the snow erosion variability over time, and its dependency on meteorological variables, particularly air temperature. Finally, we analysed the climatic sensitivity of net snow accumulation and erosion for six different scenarios of atmospheric warming and cooling.

2 Study area and data

2.1 Study area

The study area is located on Mt. Ortles (3905 m a.s.l.; 46.508°N, 10.541°E), the highest peak in the Eastern Alps, within the Ortles-Cevedale Mountain Group (Fig. 1). The Alto dell'Ortles glacier lies on the north-western slope of the mount, extending from 3018 to 3905 m a.s.l. and covering an area of 1.19 km² (2017). Ice thickness reaches up to ~75 m (Gabrielli et al., 2012), with the basal ice layers preserving a paleoclimatic record of the past ~7 kyr (Gabrielli et al., 2016, 2025). The glacier exhibits a polythermal structure, with temperate firn overlying colder ice below the firn-ice transition at ~ 30 m depth. The firn was risen to temperate conditions due to meltwater percolation, which was particularly high in some recent ablation seasons, for example during the 2003 heatwave (Beniston, 2004; Gabrielli et al., 2012).

Since 2008, this glacier has been the focus of the "Ortles Project" (ortles.org), an international research program aimed at recovering deep ice cores for paleoclimate reconstruction and collecting data for multiple cryospheric components.

Mt. Ortles is located near the inner dry zone of the Alps and is subject to a continental climate. Long-term observations from Solda (valley floor, Fig. 1) indicate a mean annual precipitation of 800–950 mm between 1981 and 2010 (Adler, 2015). On the top of Mt. Ortles, annual precipitation is estimated between 1300 and 1400 mm, based on mass balance observation conducted from 2009 to 2016 (Carturan et al., 2023). This precipitation estimate may vary significantly across space due to the influence of the wind on snow accumulation and redistribution, and to the influence of spatial variations in precipitation.

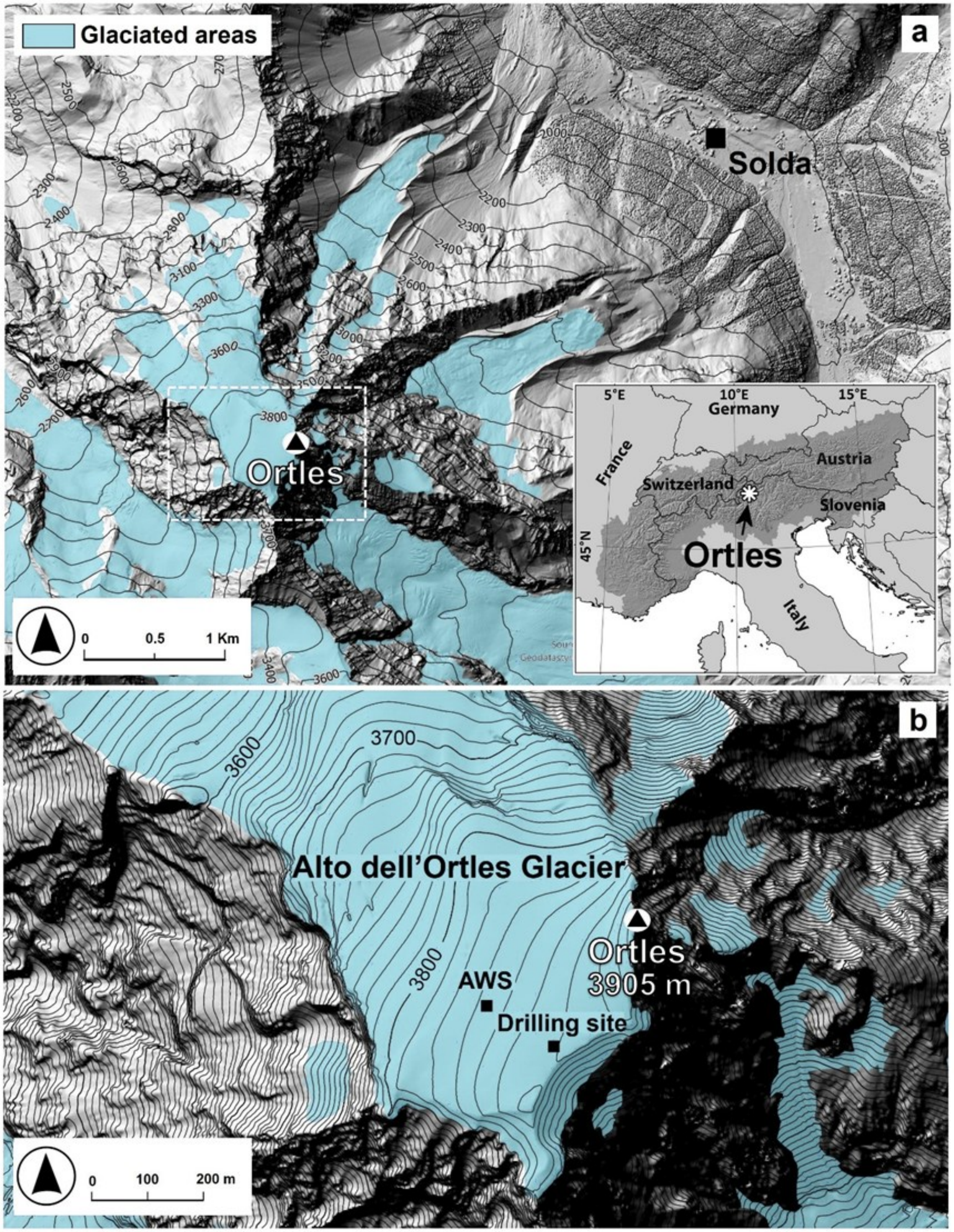

Figure 1: Location of the ice core drilling site and the automatic weather station (AWS) on Mt. Ortles. The background hill-shaded DEM (2017 lidar survey) and 2017 glaciers' outlines are from https://mapview.civis.bz.it (last access: 15 September 2025) (Agenzia per la Protezione civile, Autonomous Province of Bolzano).

2.2 Meteorological data

An automatic weather station (AWS) operated in the upper accumulation zone of the Alto dell'Ortles Glacier from September 2011 to June 2015. The solar-powered AWS was installed at 3830 m a.s.l., approximately 200 m downslope of the drilling site, and on a site with western exposure. A Campbell Scientific CR-1000 data logger stored 15-minute values coming from sensors of air temperature and relative humidity (Vaisala HMP155A), wind speed and direction (R. M. Young 05103), incoming and outgoing shortwave and longwave radiation (Delta Ohm LP Pyra 05 and LP PIRG 01), and snow depth (Campbell Scientific SR50A). Some sensors have been duplicated to provide a backup in the event of a malfunction. Details on sensors characteristics have been reported in Table 1 whereas details and pictures of the AWS can be found in Carturan et al. (2023).

Table 1: Characteristics of sensors installed at the Mt. Ortles AWS, which provided the nivo-meteorological data used in this work.

Measured variable	Sensor	Number of sensors	Initial height (m)	Radiation shield	Accuracy
Air Temperature	Vaisala HMP155A	1	3.7	R. M. Young 43502 fan-aspirated	$\pm (0.226 - 0.0028 \cdot T)$ °C
Air Temperature	Vaisala HMP155A	1	3.9	Campbell Scientific MET 21	$\pm (0.226 - 0.0028 \cdot T)$ °C
Relative humidity	Vaisala HMP155A	1	3.7	R. M. Young 43502 fan-aspirated	± (1.0 + 0.008 × reading) % RH from −20°C to +40°C, ± (1.2 + 0.012 × reading) % RH from −40° to −20°C
Relative humidity	Vaisala HMP155A	1	3.9	Campbell Scientific MET 21	± (1.0 + 0.008 × reading) % RH from −20°C to +40°C, ± (1.2 + 0.012 × reading) % RH from −40° to −20°C
Snow height	Campbell scientific SR50A-L	2	4.0		±1 cm or 0.4% of distance to target
Wind speed and direction	R. M. Young 05103	2	4.3		Wind speed: ± 0.3 m/s or 1% of reading Wind direction: ± 3°

Incoming and outgoing shortwave radiation	Delta Ohm LP Pyra 05	1	4.0		±2%
Incoming and outgoing longwave radiation	Delta Ohm LP PIRG 01	1	4.0		±2%

The AWS was mounted on an aluminium tower, composed of two-meter segments and anchored two meters deep into the snow, supported by wooden platforms at the bottom. Once installed, the tower rose 4 meters above the snow surface. Sensors and photovoltaic panels were placed on the top of the structure, while the data loggers and batteries were housed in a fiberglass box just above the snow surface. Because of the snow accumulation, the height of the sensors relative to the glacier surface varied seasonally. To ensure continuous operation and avoid sensor burial by net accumulation of snow, the tower was extended each year by adding a two-meter segment each time.

Precipitation could not be measured with reasonable accuracy at the Ortles AWS, because it would have required a heated rain gauge with too high-power demand. In addition, due to the high elevation and wind exposure, any data collected would have been highly underestimated and difficult to correct, due to the well-known issues (high wind speed, high frequency of snowfall, rain gauge perturbations of the wind field) affecting precipitation measurements in similar environments (Rasmussen et al., 2012; Kochendorfer et al, 2017). Consequently, a rain gauge was not installed at the AWS, using and scaling instead precipitation data measured at the nearest weather station in Solda (1907 m a.s.l.), operated by the local meteorological agency (Ufficio Idrografico, Provincia Autonoma di Bolzano, meteo.provincia.bz.it).

The raw meteorological data from Mt. Ortles and Solda were quality-checked and validated against observations from neighbouring weather stations (details are reported in Carturan et al. 2023), specifically Madriccio (2825 m) and Cima Beltovo (3328 m) for air temperature and wind speed, and Fontana Bianca (1900 m) for precipitation. Precipitation data from Solda were also corrected following the procedure described in Carturan et al. (2012,) to account for the rain gauge underestimation. Since the SNOWPACK model requires a continuous meteorological input in the investigated period, missing or unreliable data were reconstructed using backup sensors at the AWS when available, and data from Madriccio and Cima Beltovo weather stations in case backup sensors were unavailable or unreliable. In this case, the missing data at the Ortles AWS were calculated by means of linear regression from Madriccio and Beltovo weather stations. For wind speed and direction, data gaps (7% of the total period of observation, Table B1 in the Appendix) were filled with seasonal-mean values. Gap-filling was carried out using the MeteoIO/SNOWPACK toolchain (Bavay and Egger, 2014). The obtained final dataset is shown in Fig. 2.

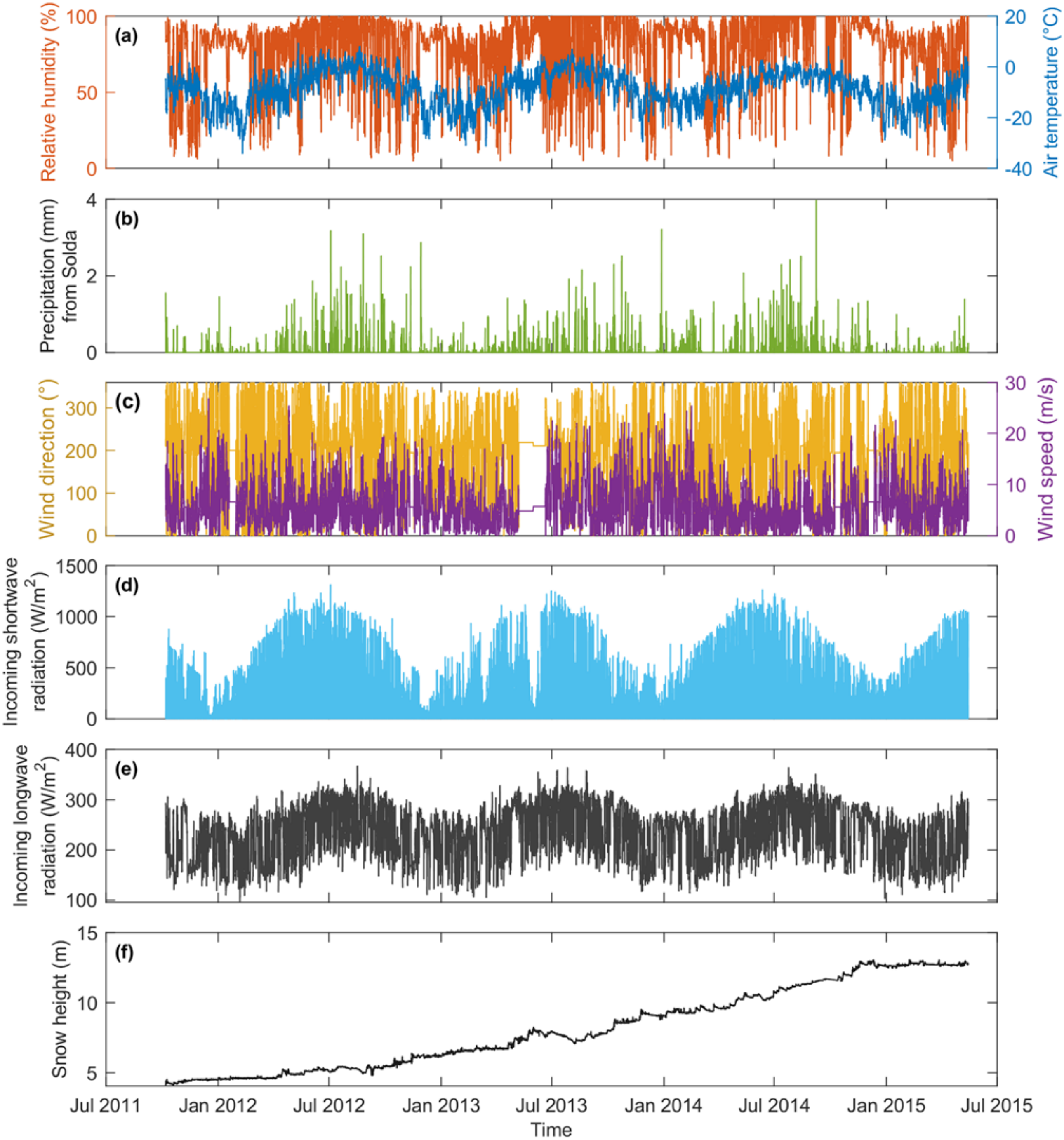

Figure 2: Hourly values of nivo-meteorological data recorded by the Ortles AWS (3830 m a.s.l.) from September 2011 to June 2015: (a) air temperature and relative humidity, (b) precipitation, (c) wind speed and direction, (d) incoming shortwave radiation, (e)

incoming longwave radiation, (f) snow height. Please note that precipitation data were not measured at the same AWS, but come from the nearby village of Solda (1907 m a.s.l.).

At 3850 m a.s.l. the mean annual air temperature is approximately -9°C. Snow accumulation occurs mainly from October to May. The melt season typically spans from June to September, though summer snowfalls are frequent on the glacier summit. The intensity and duration of ablation exhibit substantial differences from year to year and are strongly influenced by heatwaves. Rainfall is rare at these elevations, but isolated rain events have been observed on the summit over the past 15 years (Carturan et al., 2023).

In the period of direct observations, between September 2011 and June 2015, the mean monthly air temperature ranged between -17.24 and -1.63°C, peaking in August (Fig. 3a). The precipitation showed a distinct maximum in summer and a minimum in winter, which is typical of the local climate (Fig. 3b). The wind speed was highest in winter and lowest in spring and in September. The dominant wind direction was from W-SW (Fig. 3c), with significant variations considering all hours of observations (Fig. 4a), hours with precipitation (Fig. 4b), hours of erosion during precipitation (Fig. 4c), and hours of erosion after precipitation (Fig. 4d).

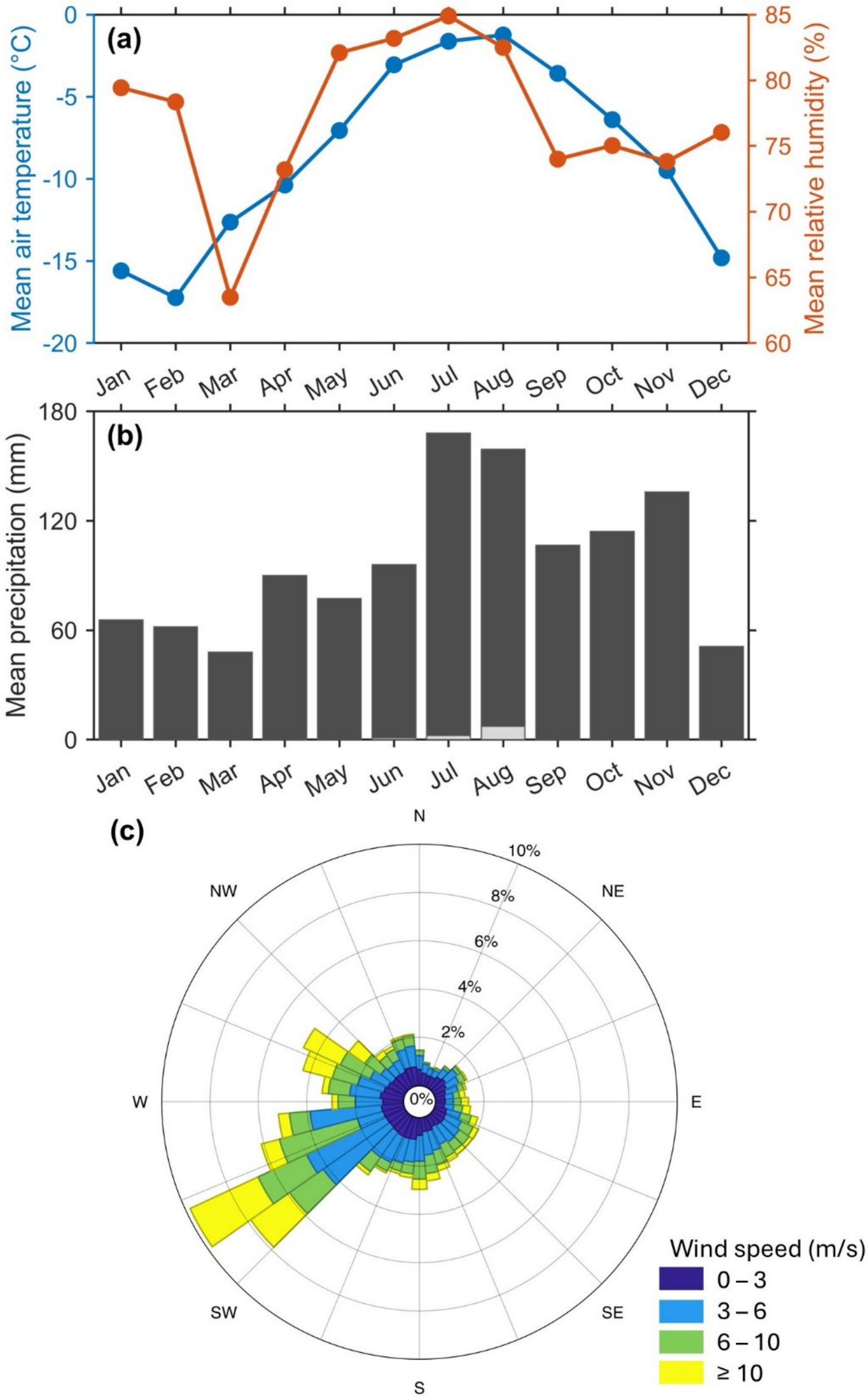

Figure 3: Monthly means of (a) air temperature and (b) precipitation in the period between September 2011 and June 2015 at the Mt. Ortles automatic weather station site (3830 m a.s.l.). The frequency distribution of wind direction and wind speed in the same

period is reported in panel (c). Air temperature and wind data come directly from the automatic weather station at 3830 m a.s.l., whereas precipitation is calculated from the data recorded at the Solda village, right below Mt. Ortles, at 1907 m a.s.l.

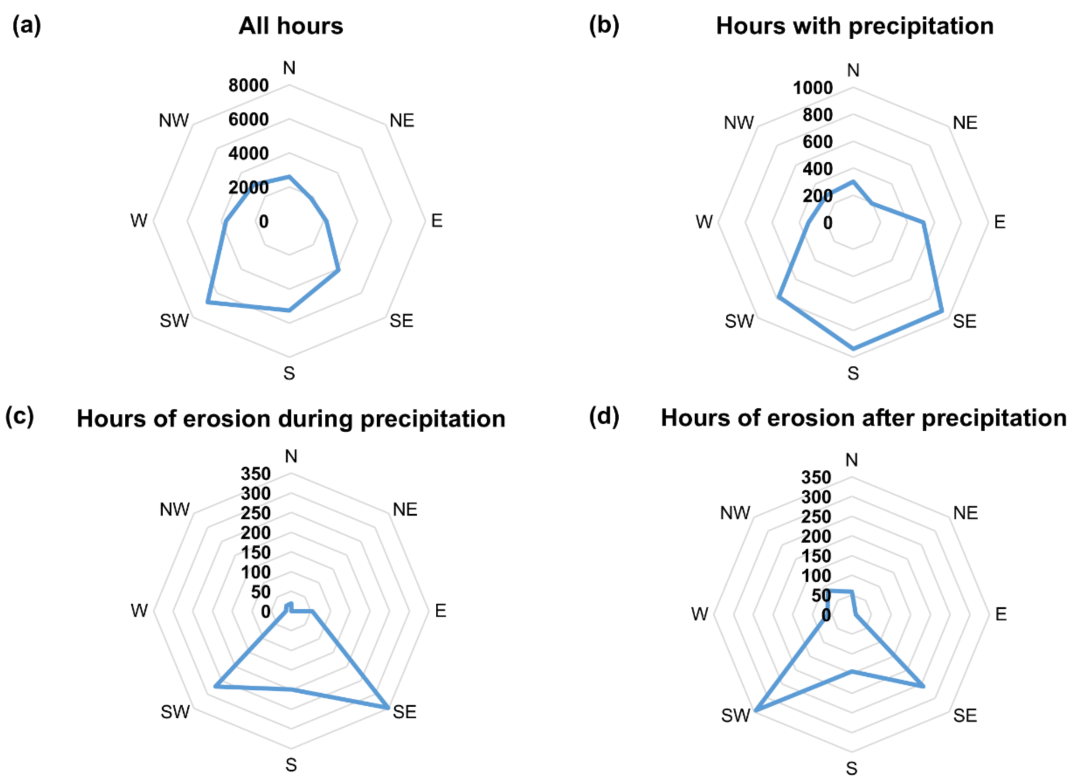

Figure 4: Frequency of wind direction for (a) all hours of observations, (b) hours with precipitation, (c) hours of erosion during precipitation, and (d) hours of erosion after precipitation.

2.3 Mass balance data

Seasonal and annual glacier mass balance measurements were carried out between June 2009 and September 2014 at the ice core drilling site and at the AWS location. Winter balance surveys were performed in June or early July before the start of the ablation season. Summer and annual balance measurements took place in late August or early September, at the end of the melt season. Field observations included snow depth probing around both sites, combined with snow and firn density measurements in snow pits dug down to the previous summer surface. Snow stratigraphic profiles were carried out along shaded pit walls, including observations of snow and firn temperature, hardness, grain type and size, and the presence of ice lenses and dust layers (Gabrielli et al., 2010). These stratigraphic observations were helpful in identifying the summer surface, both within snow pits and while probing snow depth. Density measurements were used to convert snow depth into water equivalent.

3 Methods

3.1 Snow modelling

We used the snow cover model SNOWPACK (Lehning et al., 2002a, 2002b) to calculate the energy and mass balance at the Ortles AWS site and to obtain a continuous snow water equivalent data series at the study site in the period from September 2011 to June 2015. This data series was required for this study, but could not be derived directly from snow depth data because snow density (and its variations) were unknown. Originally developed for avalanche warning, SNOWPACK is widely used to study the alpine cryosphere, including snow and glacier mass balance and mountain permafrost (Meirold-Mautner and Lehning, 2004; Obleitner and Lehning, 2004; Rasmus et al., 2004; Luetschg et al., 2008; Bavay et al., 2009, 2014). SNOWPACK is a physics-based, one-dimensional, multi-layer numerical model designed to simulate the evolution of the snow cover using meteorological data from automatic weather stations. The model simulates the stratigraphy and the microstructure of the snow by modelling energy and mass fluxes. It employs a Lagrangian finite-element method to solve the heat transfer equations. A key feature of SNOWPACK is its detailed representation of snow metamorphism, which is closely linked to mechanical properties such as the thermal conductivity and viscosity. The model also accounts for the interactions between the snow surface and the atmosphere, including radiative transfer processes such as the penetration of shortwave radiation. The surface energy exchange in SNOWPACK is detailed in Lehning et al., (2002b). A fixed roughness length of 0.002 m has been assumed together with the Holtslag stability correction in a bulk aerodynamic Monin-Obukhov formulation for the turbulent fluxes. The standard SNOWPACK parameterization for albedo has been employed.

The computational framework is based on a set of key state variables that serve as the foundation for simulating the snow microstructure and its metamorphic changes. These variables are used to derive essential bulk properties needed to solve the model core conservation equations. A detailed description of the mathematical formulations and governing equations implemented in SNOWPACK can be found in Bartelt and Lehning (2002), and in Lehning et al. (2002a, 2002b).

SNOWPACK explicitly accounts for wind-driven snow erosion through its snowdrift module (Lehning et al., 2000). The scheme first determines a threshold friction velocity (m s^{-1}) at the snow surface following Schmidt (1980), based on its erodibility calculated as a function of snow grain shape, size and bond strength (Lehning et. al, 2000). When the actual friction velocity, derived from the logarithmic wind profile including stability corrections, exceeds the threshold friction velocity, snow erosion initiates. The horizontal drifting snow mass flux is then calculated following Lehning and Fierz (2008). To translate the horizontal mass flux into a vertical surface erosion mass flux, a fetch length of 70 m is assumed, which is an arbitrary length scale under the assumption that the mass that is transported (e.g. over a mountain ridge) is then distributed along the fetch distance on the lee side (Lehning and Fierz 2008, Wever et al. 2023). At each time step, the erodibility of the surface layer is updated, allowing SNOWPACK to consistently represent erosion also during snowfall.

To run the model the following meteorological variables were used as inputs: air temperature, relative humidity, wind speed, incoming and outgoing shortwave radiation, incoming and outgoing longwave radiation and precipitation. All input data came from the Mt. Ortles AWS, with the only exception of precipitation that comes from the Solda village, as detailed in Section 2.2. The model framework relies on the MeteoIO library (Bavay and Egger, 2014) for meteorological data pre-processing. This module acts as a middleware layer between raw meteorological data and the model, pre-processing input data. Gap filling methods are mentioned in Section 2.2; in addition, the MeteoIO module adjusts input data for the varying sensor's height above the surface, based on readings from the snow depth sensor.

A point simulation of the snowpack was conducted at the AWS site using a 15-minute time step interval. The simulation began on 7 September 2011 and extended until 14 of June 2015. SNOWPACK was initialized using snow pit observations collected at the AWS site a few days before the start of the simulation. These observations extended from the glacier surface down to 400 cm and included snow and firn stratigraphy (grain size and shape), density, and the temperature profile. The snow accumulation was simulated using the Solda precipitation, corrected for gauge undercatch as explained in Section 2.2, and then adjusted using a 28% km^{-1} vertical precipitation lapse rate, obtained from 40 years of meteorological and snow water equivalent data in a nearby study site (Val de La Mare, 10 km south-east of Mt. Ortles, Carturan et al., 2019). In this way, the vertical precipitation lapse rate was derived from independent meteorological observations and was not used as a calibration parameter. A fixed lapse rate was preferred to a month-specific lapse rate (as employed by Carturan et al., 2019) because the seasonality of lapse rates is expected to vary significantly across the region, in particular during summer when thunderstorms prevail, but also considering the orographic characteristics. As we have no information on how monthly lapse rate might change in the Ortles area, compared to Val de La Mare, we consider it more appropriate to use a fixed lapse rate.

The wind speed was also adjusted by means of a multiplicative factor, to account for the fact that on top of Mt. Ortles the wind speed is not expected to follow strictly a vertical logarithmic profile as in horizontal, unobstructed terrain (Mott et al., 2010; Stiperski and Rotach, 2016). The multiplicative factor for wind speed was adjusted iteratively to minimize the Root Mean Square Error (RMSE) between measured and modelled mass balance at the simulation site.

3.2 Analysis of snow erosion

The snow erosion process was analysed in terms of snow water equivalent (SWE), rather than in terms of snow height, allowing changes due to wind redistribution to be isolated from those caused by other processes, like compaction. We excluded from analyses the periods with interpolated wind speed data (7% of the total, Table B1), to avoid introducing possible external noise to the data.

The analyses regarded hourly snow erosion events, identified using the SNOWPACK output variable MS_Wind (mm h^{-1}), which describes the mass loss during erosion. An hourly snow erosion event was identified when MS_wind exceeded 0.1 mm h^{-1}. Each hourly snow erosion event was characterized using descriptors that quantify the meteorological conditions during erosion, and the average conditions during the 'life' (abbreviation used in this study to indicate 'lifetime') of each snow layer that was removed by wind erosion (Table 2). The beginning of each layer's life was set when snow accumulation exceeded 0.1 mm h^{-1}. The duration of each new layer's life was up to the end of the simulation period, unless the layer was removed by melt, erosion, or sublimation/evaporation.

Because the mechanical response of snow to wind differs under wet and dry conditions, erosion events were classified accordingly. 'Wetted' snow was defined as snow exposed to positive air temperatures since layer formation, representing a cohesive wet regime, even if wetting was followed by refreezing of liquid water (because in that case the snow surface keeps high mechanical strength). 'Dry' snow, in contrast, was defined as snow that never experienced positive air temperatures. Based on this criterion, 1731 dry snow erosion events and 155 wetted snow erosion events were identified.

The snow erosion process was analysed using correlation and frequency distribution analyses. Two correlation matrices were calculated for dry snow and other two for wetted snow: (i) the first dry/wetted snow matrix including all hourly erosion events, and (ii) the second dry/wetted snow matrix that includes the threshold wind speed for snow erosion (WS_Th) and the temperature threshold for snow erosion (T_Th) variables, which could be calculated only when erosion starts (i.e. they could not be calculated over consecutive hourly erosion events).

Table 2: Calculated descriptors used to characterize the hourly snow erosion events.

Variable name	Unit	Explanation
WE_Eroded	mm	Total SWE eroded during the event
WS_Erosion	m s^{-1}	Wind speed during the erosion event
T_Erosion	°C	Air temperature during the erosion event
WS_Th	m s^{-1}	Wind speed threshold, defined as the mean wind speed between the hour preceding erosion and the first hour of erosion
T_Th	°C	Air temperature threshold, defined as the mean air temperature between the hour preceding erosion and the first hour of erosion
Age	h	Time since the formation of the snow layer
WS_Life	m s^{-1}	Mean wind speed since snow layer formation
T_Life	°C	Mean air temperature since snow layer formation
PDG_Life	°C	Cumulative positive degree hours since snow layer formation
MELT_Life	mm	Cumulative SWE lost by melt since snow layer formation

3.3 Sensitivity analysis of snow erosion to changes in air temperature

To assess the sensitivity of wind-driven snow erosion to changes in air temperature, we performed additional SNOWPACK simulations applying a fixed offset to the input temperature data. Six scenarios were simulated, shifting the observed air temperature data by –3, –2, –1, +1, +2, and +3 °C, relative to the baseline (i.e. the observation period from 2011 to 2015). With the word ‘scenario’ we mean a mere increase or decrease in air temperature, which is used to assess the model’s sensitivity exclusively to air temperature perturbations. This approach, even if simplified, aims to investigate the response to both colder conditions (representative of past centuries) and plausible near-future warming at high elevation in the Alps (IPCC, 2022). All other meteorological data were kept unchanged considering the lack of significant trends in long-term observation series and high uncertainty in future projections (Brunetti et al., 2009; De Blasi, 2018; IPCC, 2022), as discussed in Section 5.1. In this framework, the word 'scenario' does not refer to past or future shifts in climate conditions, which would have implied modifications in all meteorological variables.

Each experiment covered the same period as the reference run (7 September 2011 to 14 June 2015). For each scenario, we analysed the model output in terms of snow water equivalent, the change in the relative contribution of erosion, melt and net accumulation to the total mass balance, and the change in the monthly regime of snowfall erosion by wind. We included also sublimation and evaporation fluxes to assess their relevance in comparison to the other mass fluxes.

4 Results

4.1 Snowpack mass balance modelling

The RMSE between measured and modelled mass balance at the simulation site was optimized using a multiplicative factor for wind speed of 0.70. Considering all mass balance measurement sub-periods, the RMSE between measured and modelled SWE above the previous year's summer surface is 0.115 m w.e. The agreement between measured and modelled mass balance was higher in the accumulation season (RMSE = 78 mm w.e.), compared to the ablation season (RMSE = 209 mm w.e.). An average overestimation of 182 mm w.e. was detected in summer balance, which occurred mostly in 2013. The winter balance was underestimated by 52 mm w.e. on average (Fig. 5).

According to SNOWPACK calculations, 4.401 m w.e. accumulated at the study site between 17 Sep 2011 and 23 Sep 2014. The annual accumulation rate was lower in the 2011/12 balance year and higher in the 2012/13 and 2013/14 balance years, with similar rates in the latter two years. The largest part of snow accumulation occurred during the cold season (from October to March), while the warm season (from April to September) still contributed, with summer gains ranging from 0.04 m w.e. (2012) to 0.49 m w.e. (2014), whereas 2013 experienced a net summer ablation of 0.24 m w.e.

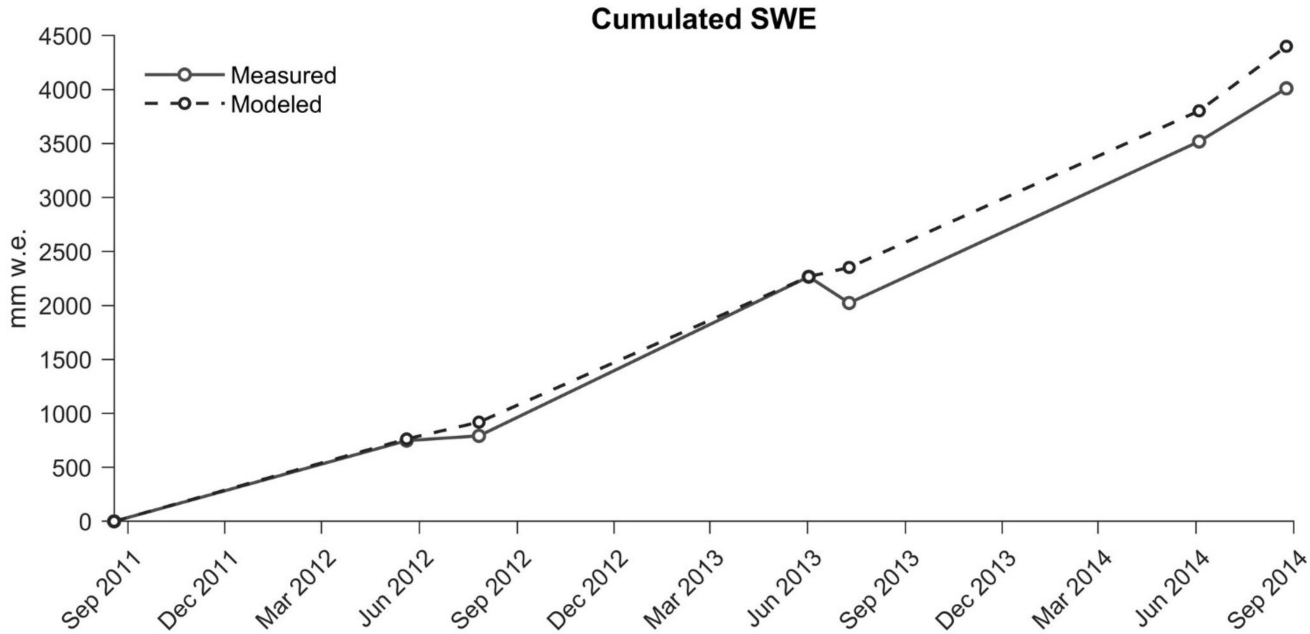

Figure 5: Comparison between modelled and measured snow water equivalent (SWE) at the Mt. Ortles AWS site.

The build up of the snowpack modelled at the Mt. Ortles AWS site from 7 September 2011 to 14 of June 2015, and the associated snow layering, is displayed in Fig. 6a. Figure 6b shows a close-up period between 13 and 17 December 2011, when several snow erosion events took place in a sub-freezing temperature regime. Two major events can be recognized: the first occurred on 13 December, after a snowfall the day before that was accompanied and followed by low wind speed. Wind erosion exclusively regarded fresh snow and was triggered when the hourly-mean wind speed rose above 10 m s^{-1}, ceasing when it fell below 12 m s^{-1}. The second major erosion event, removing 35 mm SWE (7 times higher erosion compared to the first event) was triggered when the wind speed rose above 15 m s-1 on 16 December, and was characterized by a much higher wind speed, averaging 22 m s^{-1} with hourly-mean peaks above 27 m s^{-1}. This second event eroded much older snow, including 42 days-old snow which was also wetted (even if with a very small positive degree hours equal to 1.6°C).

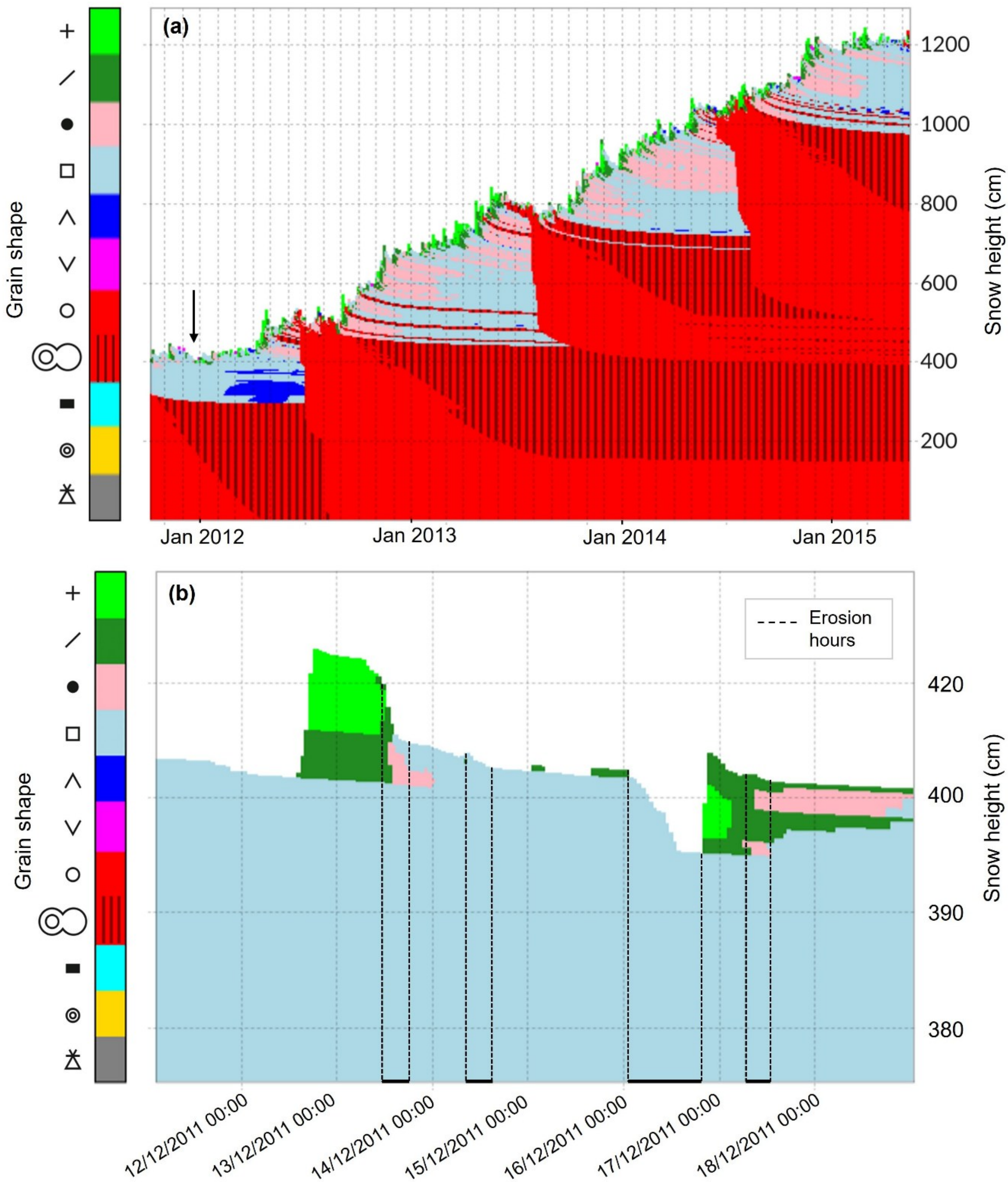

330 Figure 6: (a) Snow pack build up and evolution on the Mt. Ortles AWS site from 7 September 2011 to 14 of June 2015, modelled by the SNOWPACK model. Panel (b) shows a close-up of the snow erosion events beteen 13 and 17 December 2011, indicated by the black arrow in (a). The grain shape symbols derives from the Fierz et al., (2009) International

Classification for Seasonal Snow on the Ground.

4.2 Analysis of snow erosion

4.2.1 Correlation analysis

For dry snow, in addition to the dependency of the water equivalent eroded (WE_Eroded) on wind speed during erosion (WS_Erosion), both correlation matrices indicate that WE_Eroded was positively correlated also with wind speed since layer formation (WS_Life) and the threshold wind speed for erosion initiation (WS_Th, Figs. 7a and 7b). Interestingly, WS_Life was strongly anticorrelated with Age, suggesting that wind speed was highest during precipitation events, or shortly afterwards. Age was positively correlated with WS_Th and WS_Erosion, meaning that older snow layers required higher wind speed to start being eroded. In contrast, Age was negatively correlated with air temperature during erosion (T_Erosion) and mean air temperature since layer formation (T_life), indicating that layer persistence for long periods, before being eroded, was more likely during winter.

Even if the p-values suggest high statistical significance for correlations between the erosion rate (WE_Eroded) and temperature-related variables (T_Th, T_Erosion, T_Life, PDG_Life, MELT_Life), likely due to the high sample size, based on the very low correlation coefficients we consider WE_Eroded not meaningfully affected by these variables. This means that air temperature did not directly influence the snow erosion rate once the erosion had started. However, it strongly influenced initiation and frequency of erosion, as reported in section 4.2.2 (Figs. 8, 9 and 10).

For wet snow, the relationship between the erosion rate and the wind speed was weaker and only significant considering all erosion hours (Fig. 7c), whereas considering only hours when erosion started this relationship vanishes (Fig. 7d). Differently from dry snow, wet snow looks more affected by temperature-related variables (in particular T_Erosion, T_Life, MELT_Life). These negative correlations suggest that increasing air temperature inhibited wet snow erosion, as can expected due to a faster metamorphism of the snow surface.

As observed for dry snow, Age was positively correlated with WS_Th and WS_Erosion, meaning that older snow required higher wind speed for being eroded. Another similarity with dry snow is found in the highly negative correlation between Age and WS_Life (wind speed is highest during precipitation or shortly afterwards) and between Age and T_Erosion, T_Life and T_Th, confirming that also wet snow persisted longer in the cold season, before being eroded. The age of wet snow was positively correlated with cumulative positive degree days since layer formation (PDG_Life), suggesting that the longer a layer persisted, the higher the probability that it experienced positive temperature.

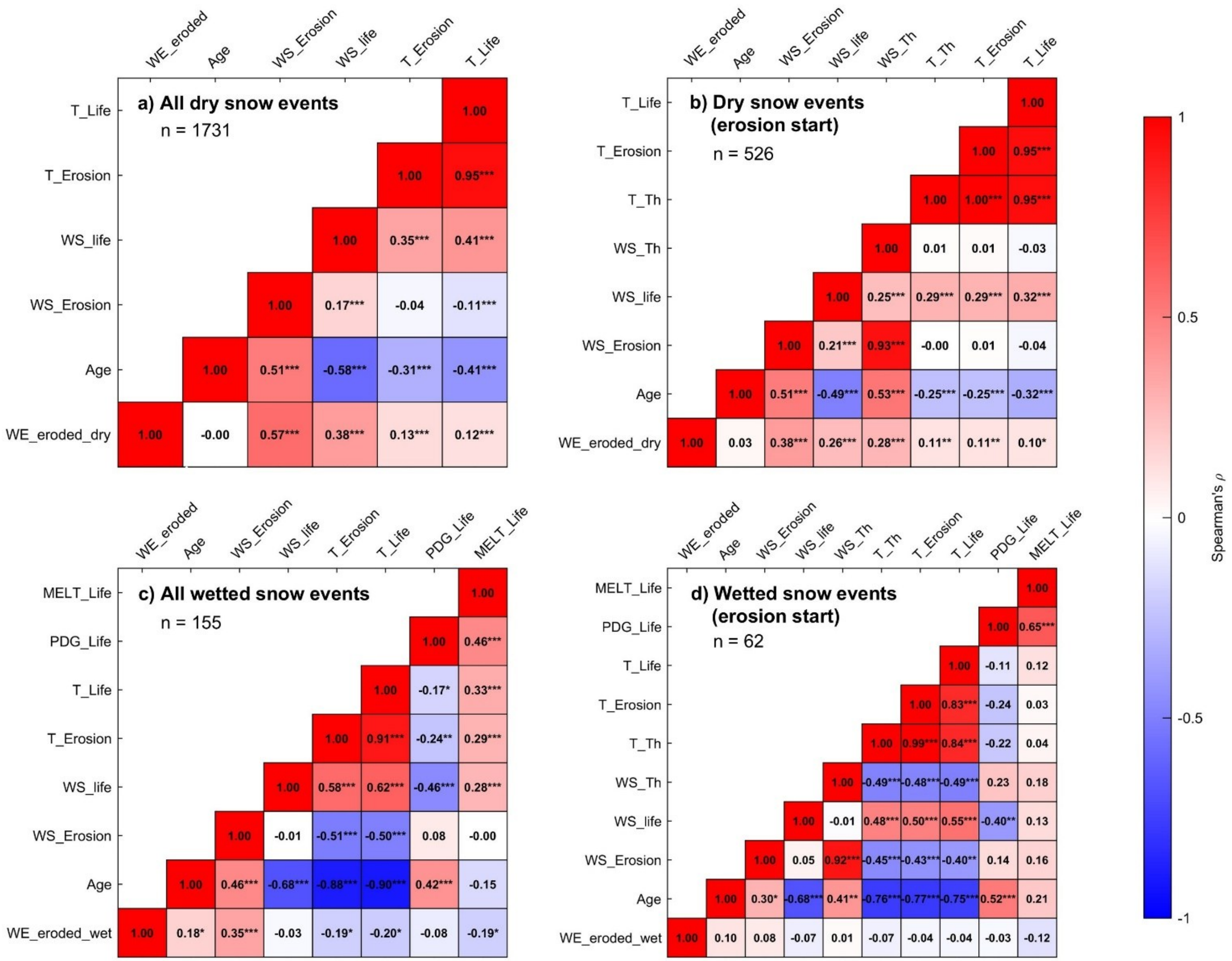

Figure 7: Spearman correlation matrix among erosion-event descriptors for (a) all dry-snow hourly erosion events, (b) dry-snow hourly erosion events, restricted to hours when erosion starts, (c) all wetted snow hourly erosion events, and (d) wetted snow hourly erosion events, restricted to hours when erosion starts. Colour encodes sign and magnitude of correlation coefficients (blue = negative, red = positive). Asterisks indicate significance (* $p < 0.05$, ** $p < 0.01$, *** $p < 0.001$).

4.2.2 Frequency distribution analysis

The cumulative relative frequency distributions of snow erosion events and cumulative relative SWE eroded were analysed as a function of layer age to assess when the largest amount of snow erosion took place. The analysis shows that erosion occurred predominantly soon after deposition (Fig. 8). Considering dry and wetted snow erosion together, 50% of the total SWE was eroded within the first 6 h, 66% within 24 h, 76% within 48 h and 90% within 240 h. Dry snow erosion was even faster, with 70% of SWE eroded within 24 h, and 95% within 240 h. In contrast, wetted snow erosion was slower: only 22% of SWE was eroded within the first 24 h, and 50% within 240 h. The cumulative relative frequency distributions of snow erosion events and cumulative relative SWE eroded as a function of layer age are very similar, except for wet erosion events that were characterised by a higher relative cumulative frequency of (small) erosion events up to 950 hours of snow layer age. The peculiar shape of the wetted snow chart is influenced by the relatively smaller sample size (155 hourly erosion events) compared to dry snow (1731 hourly erosion events). In particular, the sudden increase of WE eroded at layer age between 900 and 1000 hours depends on the erosion of an old snow layer which re-emerged at the surface and was removed during a high wind speed event (wind speed exceeding 27 m s^{-1} on 16-12-2011). In the analysed period, dry snow erosion amounted to 1091.7 mm w.e. whereas wetted snow erosion amounted to 113.1 mm w.e. Overall, dry snow erosion accounted for 91% of the total modelled erosion.

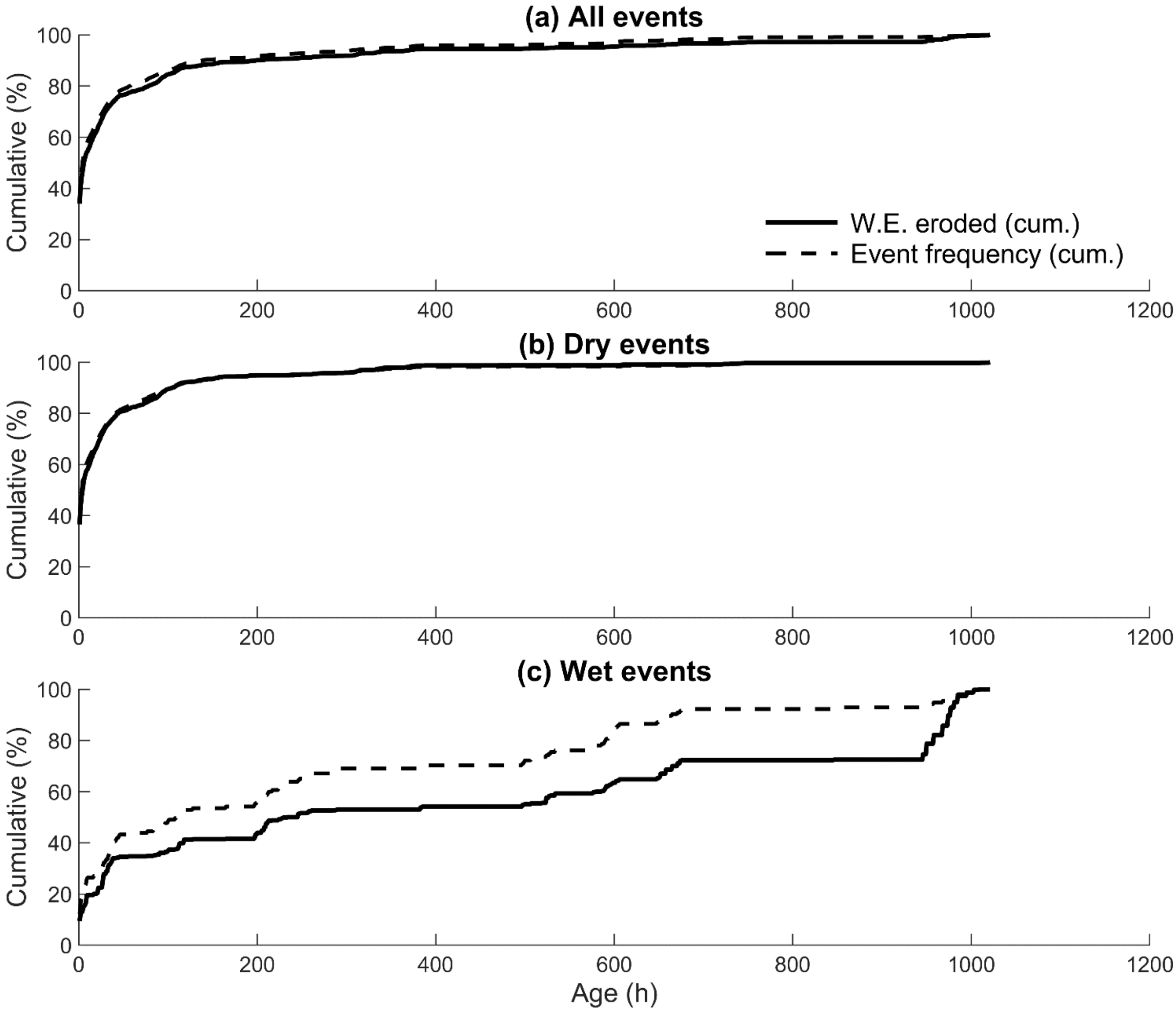

Figure 8: Cumulative relative frequency distributions and cumulative relative SWE eroded as a function of layer age. Panels show (a) all events, (b) dry snow events, and (c) wetted snow events.

Fig. 9a shows that modelled erosion occurred more frequently with dry snow at the surface, compared to wetted snow. Because the frequency displayed in Fig. 9a is affected by the fact that dry snow conditions at the surface were much more common than wetted snow conditions (82% vs. 18%, respectively), we analysed the relative frequency of snow erosion per wind speed classes, dividing hours with erosion by all hours at that wind speed and at the same time dry or wetted snow at the surface (Fig. 9b). This normalization confirms that dry snow was more easily eroded than wetted snow (three times more frequently at the same wind speed, on average), and highlights a clear pattern of increasing frequency of erosion with increasing wind speed, as expected. The SWE eroded peaks at a wind speed of 13 m s^{-1} for dry snow and between 16 and 21 m s^{-1} for wetted snow (Fig. 9c). The SWE eroded peaks at larger wind speed that the frequency of snow erosion (Fig. 9a) because at low wind speed there was frequent erosion of small quantities of snow, whereas to remove a larger amount of snow higher wind speed was required.

Fig. 10a compares the hours with erosion to the total number of hours at a given wind speed (without distinguishing between dry and wetted snow), highlighting that dry snow erosion was negligible up to 8-9 m s^{-1} and wet snow erosion became relevant only above 13-14 m s^{-1}. Fig. 10b shows that for dry snow the frequency of wind erosion was highly variable and decreasing towards 0°C. Wetted snow erosion was negligible below -1°C, likely due to refreezing, and peaked between 0 and +1°C. In both cases, the frequency of snow erosion dropped to zero above +1°C.

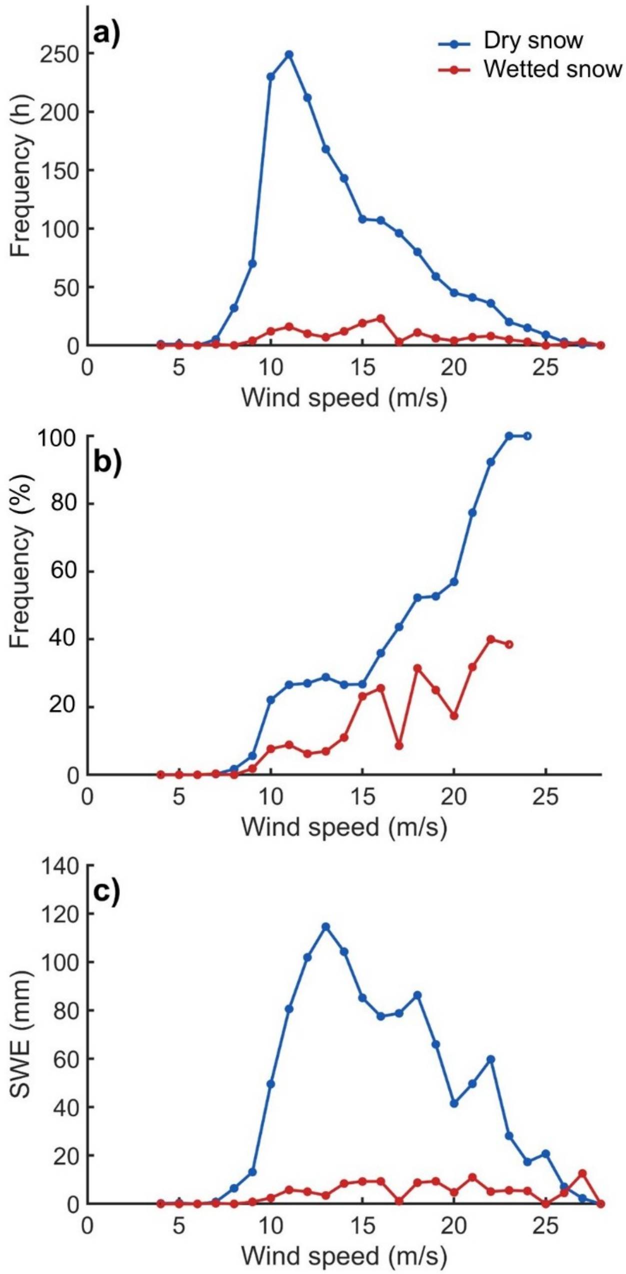

Figure 9: (a) Frequency (hours) of wind speed during modelled erosion for dry snow and wetted snow; (b) relative frequency of wind speed during modelled erosion for dry snow and wetted snow (hours with erosion divided by all hours at that wind speed and at the same time dry or wetted snow at the surface); (c) total SWE (mm) eroded per wind speed class for dry and wetted snow.

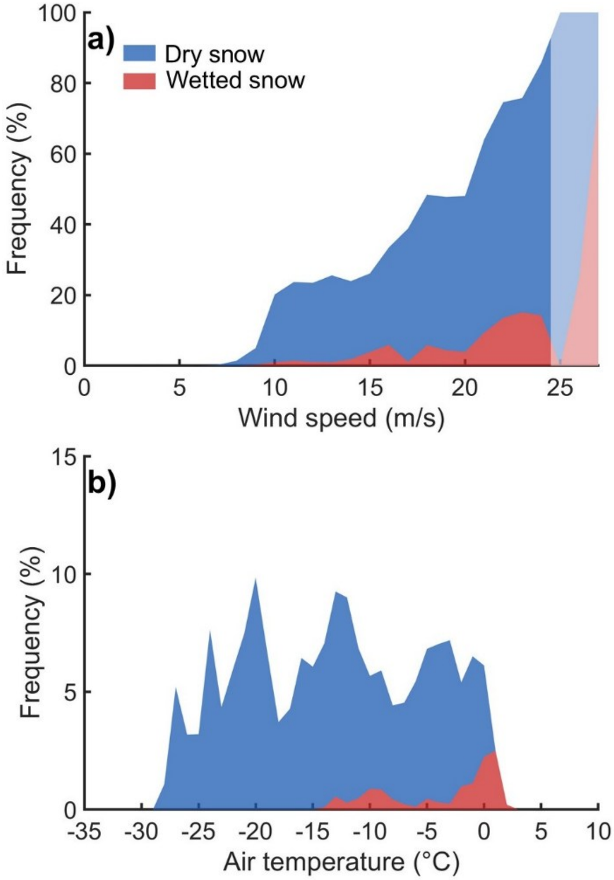

Figure 10: (a) Stacked area graph showing the relative frequency of occurrence of snow erosion for dry and wetted snow at various wind speeds (hours with erosion divided by all hours at that wind speed; wind speed ≥ 25 m s⁻¹ is shown with partial shade because the sample size was smaller than 10 hours); (b) stacked area graph showing the relative frequency of occurrence of snow erosion for dry and wetted snow at various air temperatures (hours with erosion divided by all hours at that air temperature; air temperature bins with sample size < 10 hours are not shown).

Figure 11 shows the combined effect of wind speed and air temperature on the frequency of wind erosion events (dry and wetted snow together). It is clear that most of the erosion events occurred in the upper left corner of the scatterplot, that is at a temperature relatively close (but not above) the freezing point combined with a wind speed between 9 and 15 m s^{-1}.

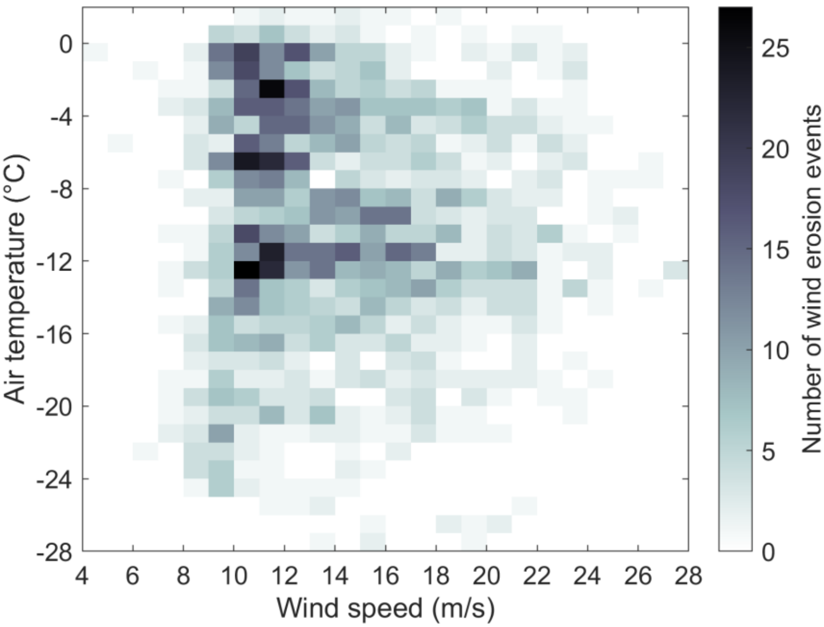

Figure 11: Two-dimensional scatterplot showing the frequency of wind erosion events (dry and wetted snow, color coded) for bins of air temperature and wind speed.

4.3 Sensitivity analysis of snow accumulation and erosion to changes in air temperature

In the period between 2011 and 2015 (baseline conditions), the mass balance was dominated by snow accumulation and wind erosion, which removed 20.9% of the total accumulated snow. Melt was comparatively less important and removed only 2.9% of total snow accumulation (Table 3). Evaporation and sublimation removed 326 mm (5.5% of total snow accumulation), whereas condensation and inverse sublimation added 43 mm, giving a net flux of -283 mm (-4.7% of total snow accumulation). The sensitivity of SNOWPACK simulations to the simulated temperature changes was remarkably higher for warming scenarios, compared to cooling scenarios. (Fig. 12). The modelled mass balance was little affected by warming up to 1°C above baseline conditions, which caused a decrease of 11.5% in the final SWE. However, a larger warming had a much stronger impact, causing a 38.5% smaller final SWE for 2°C warming, and a 71.8% smaller final SWE for 3°C warming. In contrast, cooling scenarios produced a minor increase of 0.4% in the final SWE for a 1°C temperature decrease, whereas the final SWE decreased under larger cooling (−2.2% for 2°C cooling and −3.8% for 3°C cooling).

Up to 1°C warming, wind erosion (represented by black vertical bars in Figure 12) remained dominant in removing accumulated snow (18.7%) over melt (12.5%, represented by red vertical bars in Figure 12). Larger warming implied strong melt increase and a significant decrease in the relevance of snow erosion (16.5% and 14.9% of the total accumulation for 2°C and 3°C warming, respectively). On the other hand, melt decreased almost to zero with 1°C cooling, whereas the share of total snow accumulation removed by wind erosion increased about 2% for each degree of cooling, reaching 27% for the -3°C scenario. Fluxes related to water vapor showed a lower sensitivity to changing temperature scenarios. Evaporation and sublimation losses increased by 1.2% under the largest cooling scenario, and decreased of the same amount under the largest warming scenario. Changes in condensation and inverse sublimation were negligible and reached a few tenths of a percent.

For baseline conditions, the seasonal regime of snow erosion (Fig. 13) was characterised by a prominent maximum in winter months, when 48% of monthly snowfall was eroded on average, and a minimum in spring, when 11% of monthly snowfall was eroded on average. In summer and fall, the wind erosion averaged 16% and 17% of the monthly snowfall (Fig. 13, Table A1). The highest sensitivity of wind snow erosion to warming temperature was found in spring and fall, with a maximum decrease of about 61% in March for the +3°C scenario. High sensitivity was calculated in mid-summer, whereas lower sensitivity is visible in the coldest months. On the other hand, colder temperatures affected mainly the months of May, August, September and November. In particular, for August a nearly doubling of wind erosion was calculated for the -3°C scenario. The sensitivity was smaller during winter months and in April and June.

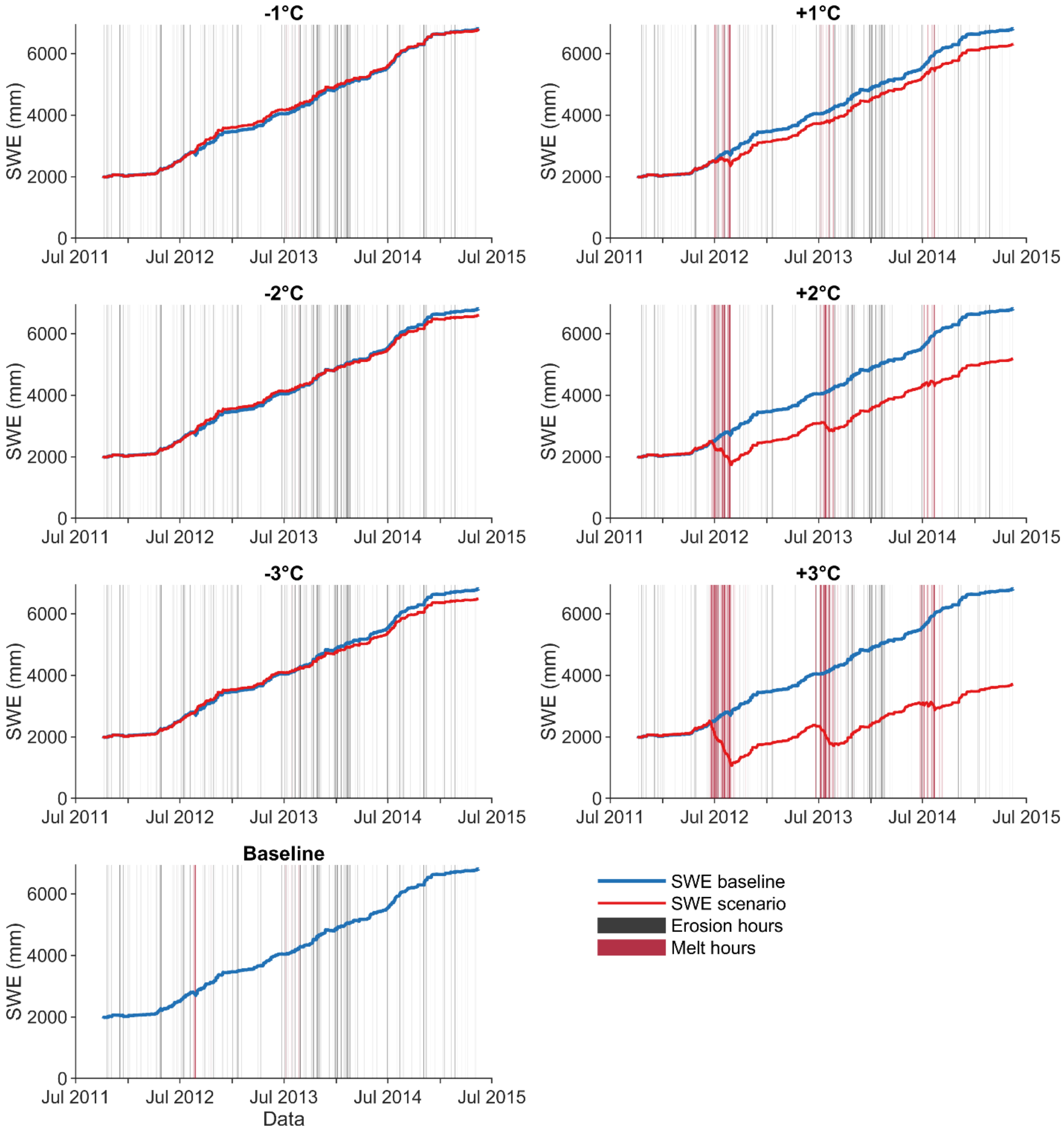

Figure 12: Modelled SWE at the AWS site for the baseline and temperature change scenarios (-3°C to +3°C). Vertical bars indicates melt and erosion hours.

Table 3. Total cumulative mass fluxes modelled for baseline and temperature change scenarios (−3 °C to +3 °C).

Variable	Baseline	−1 °C	−2 °C	−3 °C	+1 °C	+2 °C	+3 °C
Total precipitation (mm)	6142	6142	6142	6142	6142	6142	6142
Total snowfall (mm)	5978	6006	6013	6022	5864	5497	5135
Total snowfall (%)	97.3	97.8	97.9	98.1	95.5	89.5	83.6
Total erosion (mm)	1248	1396	1535	1624	1099	909	766
Total erosion (%)	20.9	23.3	25.5	27.0	18.7	16.5	14.9
Total melt (mm)	174	38	20	14	734	1785	3085
Total melt (%)	2.9	0.6	0.3	0.2	12.5	32.5	60.1
Total evaporation and sublimation (mm)	326	371	396	405	291	252	220
Total evaporation and sublimation (%)	5.5	6.2	6.6	6.7	5.0	4.6	4.3
Total condensation and inverse sublimation (mm)	43	36	32	27	48	53	59
Total condensation and inverse sublimation (%)	0.7	0.6	0.5	0.5	0.8	1.0	1.1
Net accumulation (mm)	4272	4238	4093	4006	3788	2604	1123

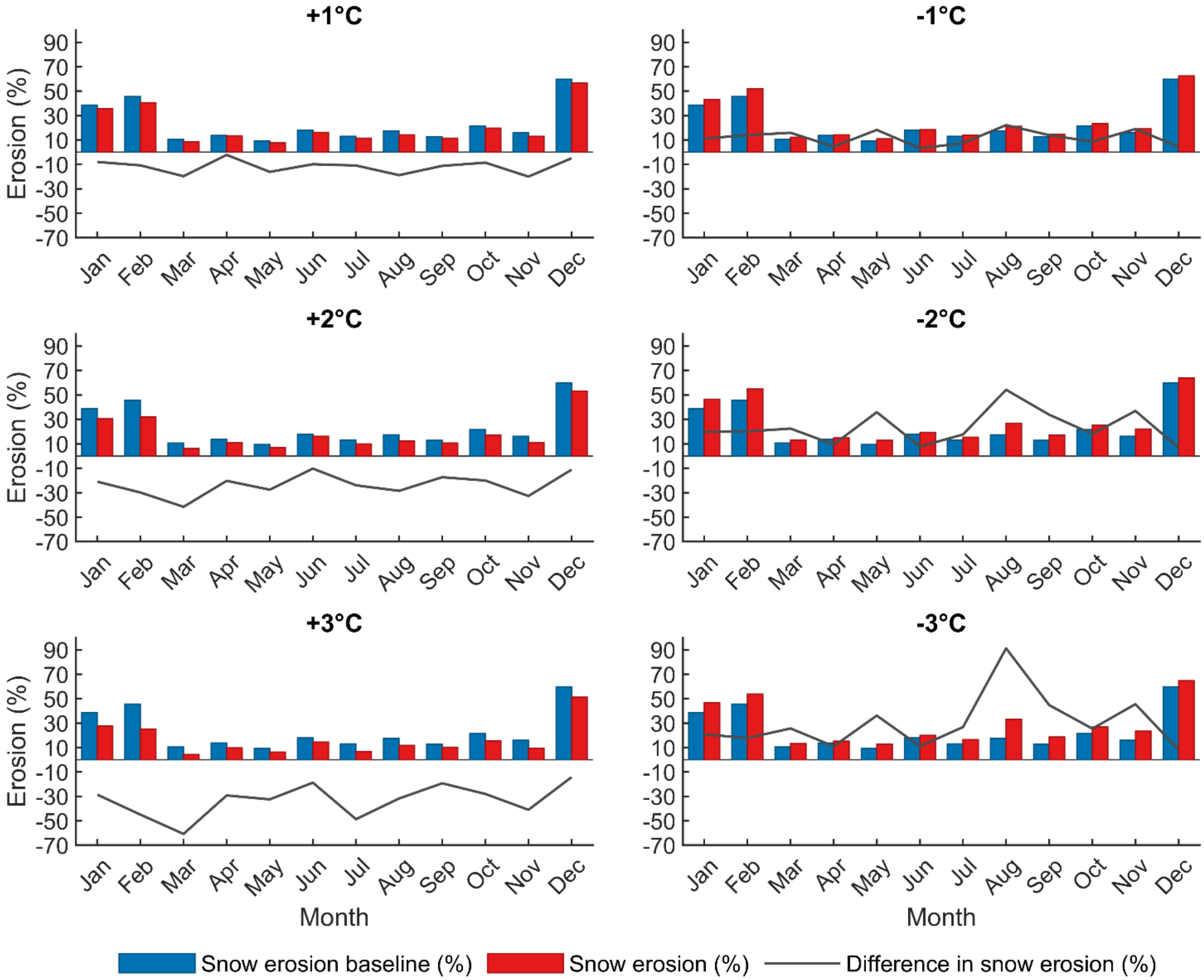

Figure 13: Modelled monthly snow erosion (percentage of monthly snow accumulation) for the baseline and temperature change scenarios (−3 °C to +3 °C).

5 Discussion

5.1 Inaccuracies and limitations

In this work, we used the model SNOWPACK to investigate the snow erosion on top of the Alto dell'Ortles glacier, based on mass balance and nivo-meteorological observations collected between 2011 and 2015. It was not possible to analyse the snow erosion directly from the data collected by the snow-depth sensors, because several other processes are involved in snow depth variations, such as sublimation, melt, compaction, and because the density of the surface layers is unknown. This made impossible to quantify erosion mass fluxes just from automatically measured snow depth and required the application of a physics-based model, constrained by field measurements, to disentangle snow erosion from other processes.

The SNOWPACK model reproduced well the measured mass balance variability across four years at the study location, once the wind speed had been adjusted to account for deviations from smooth, logarithmic profiles over complex topography (Panofsky and Ming, 1983), and the precipitation measured at the valley floor had been corrected for rain gauge errors (Carturan et al., 2012) and for the vertical lapse rate.

The requirement for a precipitation vertical lapse rate is justified by the orographic enhancement of precipitation due to the forced orographic uplifting of air masses on windward slopes of mountain ranges, which enhances the condensation of water vapor and the precipitation (e.g., Roe, 2005; Houze, 2012; Avanzi et al., 2021).

Similarly, the adoption of a multiplicative factor of 0.7 (reduction factor) for the measured wind speed is physically consistent with knowledge on wind speed-up effects over mountain tops and ridges (Jackson and Hunt, 1975; Raderschall et al., 2008). On Mt. Ortles, the wind sensor was exposed to a higher relative speed-up effect than what occurred close to the snow surface. Literature reports speed-up ranging between 30-100% in these settings compared to the logarithmic wind profile, with a maximum speed-up effect occurring within the first few meters above the ground, which is where the wind sensor was located at the study site (Taylor et al., 1987; Pellegrini and Bodstein, 2004).

In absence of higher time resolution snow water equivalent data from the field, we adopted constant values for the precipitation laspe rate and for the wind multiplier. Consequently, despite the overall good performance the model, it is possible that the model was affected by the time invariance of the two parameters for single events or periods of simulation.

For example, there is very good correspondence between modelled and measured seasonal balances (Fig. 5), except for summer 2013, when the model overestimated the mass balance by 0.33 m w.e. In this case, SNOWPACK calculated too much snowfall on Mt. Ortles, which increased surface albedo and inhibited melt. This was due to the seasonal variability of the precipitation lapse rate and type of precipitation. In summer, the study site is mainly affected by local convective precipitation (thunderstorms) that are scattered by nature, making precipitation variability more randomly distributed and less correlated with elevation when compared to frontal precipitation, which is more sensitive to orographic uplift (Adler et al., 2015). Using a constant precipitation correction factor led to significant overestimation of summer snowfall and mass balance in 2013, however possible errors in 2013 mass balance measurements in the field cannot be ruled out as well.

Low accuracy affecting mass balance measurements on Mt. Ortles can be mostly related to the difficult detection of the previous year's summer surface during snow depth soundings. The related deviation from the true value can be potentially large (up to 0.5 m w.e.) but was significantly reduced by regularly digging pits into snow and firn, which enabled detection of the previous year's summer surface with good confidence based on observations of grain shape and size, dust layers and melt/refreeze crusts. This check excluded large uncertainties in the evaluation of the annual snow depth. However, it could not completely remove inaccuracies linked to the spatial variability of snowpack thickness and density. Overall, we estimate a random uncertainty of 0.1 m w.e. per mass balance measurement, which lies within the range reported in literature for measurements under similar conditions (Zemp et al., 2013).

Inaccuracies in nivo-meteorological variables measured by the AWS may also have contributed to the total uncertainty of the model's output. Considering these sources of possible uncertainty (Sect. 3.1) and the extreme environmental conditions at the study site, the RMSE between measured and modelled seasonal and cumulated balance (0.115 m w.e.) looks acceptable. However, we preferred to remove from the presented model results periods with data gap filling to minimise external and spurious sources of variability in the modelled SWE series and snow erosion events analysed in this work, while still preserving a sample size that was sufficient for attaining statistical significance.

Using simple scenarios of changed air temperature is a simplification of future warmer climates (e.g., Dumont et al., 2025) and is mainly intended to assess the model's temperature sensitivity, as outlined in Section 3.3. However, a change in air temperature represents the main effect as climate models predict small changes in other meteorological variables such as precipitation or radiation (Kotlarski et al., 2023). The main additional effect of a warmer atmosphere in the surface energy balance is through increased longwave incoming radiation, which is captured in our simulations as this forcing is parameterised in SNOWPACK (Schmucki et al., 2015). Relative humidity can be assumed unchanged as suggested by secular meteorological observations at high elevation in the Alps showing the absence of clear trends (Brunetti et al., 2009). In addition, a minor (2-4%) decrease in relative humidity is indicated by future projections at the end of the 21th century in the European Alps (Gobiet et al., 2014), but they are highly uncertain due to the relationship between the relative humidity and precipitation, and to the high uncertainty in future trends of precipitation in the study area (Kotlarski et al., 2023; Pepin et al., 2025).

A possible limitation of the study is the relatively short observation period. This may affect, for example, the representativeness of threshold wind speed values for wetted snow erosion (due to the smaller sample size compared to dry snow), or the robustness of monthly erosion regimes (which fluctuate due to the existence of single months with unusual meteorological behaviour). Nevertheless, in view of how rare this high-elevation four-year dataset is, we consider it suitable to characterize the key processes affecting snow erosion and its temperature sensitivity at the study site.

5.2 Snow erosion and its sensitivity to air temperature

At the Mt. Ortles AWS site and during the investigated period, snow erosion played a relevant role in regulating the surface mass balance, removing 21% of the total accumulated snowfall. Snow erosion (associated with sublimation of drifted snow, Table 3) represented the dominant ablation process at this site, whereas melt only removed 2.9% of the accumulated snow during the modelled period. The western exposure enhanced snow erosion, as it frequently resulted in the AWS site lying on the windward side of the mountain (Figs. 1, 3c and 4a). Several other studies documented the importance of wind exposure of mountain slopes compared to dominant regional wind fields, as a direct control on local snow accumulation and location of glacier accumulation areas (e.g. Humlum, 1987).

Snow erosion was also promoted by high elevation, which resulted in air temperature below the freezing level most of the time (Fig. 2a). Air temperature had a dominant effect on the susceptibility to snow erosion at the glacier surface, because it was directly related to snow metamorphism and, in particular, to the formation of bonds between snow crystals and of melt-and-refreeze crusts. Dry snow was consequently more frequently eroded when compared to wetted snow, regardless of the wind speed causing drifting (Fig. 9). Above 0°C snow erosion becomes negligible (Fig. 10b).

The threshold wind speed for the initiation of erosion was highly dependent on the snow thermal regime. A wind speed of about 8-9 m s^{-1} was required to achieve a frequency of dry snow erosion significantly above zero, while this nearly doubles for wetted snow (Fig. 10a). -These values lie towards the upper end of the range reported in literature, which is between 4-11 m s^{-1} for dry snow and 7-14 m s^{-1} for wet snow (Li and Pomeroy, 1997). The high threshold wind speed on Mt. Ortles may depend on the high wind speed during precipitation (6.7 m s^{-1} on average), which increased the density and cohesion of fresh snow during deposition (Liston et al., 2017).

Precipitation events represent a source of ice particles that can create initial saltation and consequently a lower threshold for wind transport (Schmidt, 1980). This process was likely responsible of the high amount of snow erosion calculated during precipitation at the Mt. Ortles AWS. Indeed, more than half of the snow erosion occurred during precipitation (53%), or shortly afterwards (Fig. 8). This was somehow unexpected because during precipitation the atmospheric wind flow in this region is mostly from South or South-East (Fig. 4b), creating lee-side conditions at the AWS site. In fact, most wind erosion was expected to occur during northerly windstorms that frequently follow atmospheric disturbances in this region, especially during winter. In contrast, a prevailing wind erosion by south-easterly or south-westerly winds occurred, during or shortly after weather disturbances (Fig. 4c and d) and well before the wind rotation to north (generally associated with the end of the precipitation events).

Snow erosion on Mt. Ortles was mostly a winter phenomenon, due to the combination of high wind speed and low temperature. On average, 48% of the accumulated snow was removed by erosion in winter, whereas this amount ranged between 10% (in March and May) and 21% (in October) during the other parts of the year. The monthly regime of precipitation, with a maximum in the warm season (Fig. 3b), was more favourable to snow preservation than it could have been if precipitation were equally distributed over the year, or with a winter maximum. Under these conditions, the AWS site would have experienced a significantly lower annual snow accumulation.

The sensitivity of snow erosion to temperature fluctuations is expected to be highest on climates characterized by a summer maximum in precipitation, like on Mt. Ortles, because of the proximity of air temperature to the melting point. Our calculated monthly estimates confirm the highest sensitivity of snow erosion during the warm and transition seasons, and low sensitivity during winter when air temperature is far from the melting point, even under the +3°C scenario (Fig. 13).

Based on the reported 2 ± 0.3°C warming experienced by the European Alps since 1850-1900 (Dumont et al., 2025, and references therein), the -2°C scenario should represent thermal conditions in the second half of the 19^{th} century. Compared to that colder period, current conditions lead to a calculated reduction of snow erosion by 22% (29% for a thermal depression of

3°C) (Fig. 12, Table 3). At the same time melt increased only from 0.2-0.3% to 2.9% of the total accumulated snowfall. Therefore, based on these calculations, the reduced snow erosion with increasing temperatures acted as negative feedback, increasing the annual accumulation rate at this site. Our calculations thus confirm the negative feedback deriving from a moderate temperature increase, which could increase the annual accumulation rate at high elevation in the Alps, as suggested for example by Haeberli and Alean, (1985).

A further small increase in air temperature compared to baseline conditions is expected to strongly overcome this negative feedback in the near future (IPCC, 2022). With just 1°C additional warming (already partially occurred since 2015 (Jaquemart et al., 2024)), there would be more than a fourfold increase in melt and only a 2% decrease in snow erosion. When combined with a 2.5% decrease in the fraction of solid precipitation, this would result in a significant decrease in the annual accumulation rate (Table 3, Fig.12). Therefore, a 'tipping point' for the wind erosion feedback is approaching at the AWS site. It is also worth noting that areas at lower elevation with similar or higher exposure to wind erosion probably already experienced this critical temperature increase in the last decades and quickly transitioned from an erosion-dominated to a melt-dominated mass balance regime.

This study highlights and quantifies the high sensitivity of glacier mass balance to snow erosion, and of snow erosion to air temperature fluctuations, at this specific study site. These interactions may lead to a non-linear response of glacier mass balance to climate change, and to negative feedbacks that should be taken into account when projecting the future behaviour of similar, high elevation and wind exposed glacierized areas. Comparable interactions are likely to occur also in non-glacierized areas, affecting for example the thermal regime of the ground and the behaviour of the underlying permafrost.

We conclude that snow erosion processes and feedbacks should also be considered when paleoclimatic data recorded in the alpine cryosphere are used for reconstructing past environmental conditions such in the case of ice cores retrieved from high elevation glaciated areas with characteristics similar to the one analysed in this study. Like melt, wind erosion is potentially effective in removing a large fraction of the seasonal accumulated snow. On Mt. Ortles, this can occur especially during the coldest months, which are also the driest and windiest. In this case, for instance, a significant fraction of the isotopic winter signal might be missing from the Ortles ice core records. In addition, it is likely that during colder climatic phases, such as the Little Ice Age, an even lower winter 'imprint' is preserved in ice cores, because wind erosion increases at lower temperature. For these reasons, we argue that proxy system models aimed at improving dating and interpretation of ice cores, could benefit from the inclusion of simple parameterizations of snow erosion, in addition to melt (e.g. Carturan et al., 2025). This refinement looks essential for a realistic modelling of the formation and preservation of paleoclimatic proxies such as the isotopic signal and its changes through time.

6 Conclusions

In this study, we used the physics-based SNOWPACK model to investigate wind-driven snow erosion at a study site located at 3830 m a.s.l. on Mt. Ortles, in the Eastern Italian Alps, in close proximity to an ice core drilling site (Gabrielli, 2012). The model accounts for all processes and meteorological variables (including air temperature) that affect the metamorphism of snow and its susceptibility to be transported by wind. The innovative aspect of this work was the quantification of the snow erosion process and its relationship with air temperature fluctuations, differentiating between dry and wetted snow over several winter seasons, and complementing it by a sensitivity analysis with respect to temperature.

The model was run using high time resolution meteorological data collected by an automatic weather station that was operated between 2011 and 2015, combined with detailed mass balance observations carried out during the same period.

The results highlight that snow erosion by wind was a principal factor affecting the mass balance at this high-elevation site, because it removed 20.9% of the total snowfall when compared to 2.9% removal by melt. Therefore, under the climatic conditions during the study period, wind-driven snow erosion represents the dominant ablation process at the study site of Mt. Ortles at 3830 m a.s.l.

Statistical analyses revealed an inverse relationship between air temperature and total snow erosion, because cold and dry snow was more susceptible to erosion when compared to wetted snow. Overall, in the considered period, dry snow erosion accounted for 91% of the total erosion, whereas wetted snow erosion accounts for the remaining 9%. At the same wind speed, the dry snow is eroded three times more frequently than wetted snow. Once the air temperature rose above the freezing point, wind-driven erosion became negligible.

For these reasons, snow erosion on Mt. Ortles was most effective during winter, when it averaged 48% of the accumulated snow due to the interplay between high wind speed and low temperature. In the remaining part of the year, this amount ranged between 10% (in March and May) and 21% (in October).

Sensitivity analyses showed that at 3830 a.s.l. on Mt. Ortles atmospheric warming leads to a significant decrease in the total snow erosion, which can be quantified in a 2% reduction in the amount of eroded snowfall per 1°C of warming. Sensitivity was maximum in the warm season, reaching a 90% increase of snow erosion in August for a 3°C cooling, due to the higher proximity to the freezing point when compared to winter months.

Assuming a temperature increase of 2-3°C since the pre-industrial period, we calculated a 4.6-6.6% decrease in snow erosion (22-29% reduction in the eroded fraction of the total accumulated snowfall) and a 2.6-2.7% increase in melt. So far, this represented an important negative feedback at the study site, which, based on model results, experienced an increase in net accumulation. However, an additional 1°C atmospheric warming would be sufficient to overcome this negative feedback, because this site is approaching a transition from the erosion-dominated to a melt-dominated regime.

Although site-specific, these findings have broader implications for long-term glacier mass balance studies and, in particular, for paleoclimatic reconstructions from ice core data. Because wind erosion can remove a remarkable fraction of the seasonal snow signal, especially in winter, and because the efficiency of this process is likely to have varied over past decades/centuries in response to temperature fluctuations, we suggest considering this process in climatic and environmental reconstructions from ice core data. Explicitly accounting for snow erosion (in addition to melt), in the development of proxy system models will help to interpret the paleoclimatic signal preserved in alpine ice core archives.

Even if the results regard a location on a high-elevation glacier, and thus have specific relevance for the glaciological and the ice-core scientific communities, they might be of interest in other fields, such as permafrost, seasonal snow, water resource management or environmental studies.

APPENDIX A: Modelled monthly results for different air temperature scenarios

Table A1: Modelled monthly precipitation, snowfall, erosion, and melt (in mm and %) for the baseline scenario. Percentages are relative to total monthly precipitation.

Month	Precipitation (mm)	Snowfall (mm)	Snowfall (%)	Erosion (mm)	Erosion (%)	Melt (mm)	Melt (%)
January	399.02	391.64	98.15	151.66	38.72	0.00	0.00
February	389.98	382.58	98.10	174.64	45.65	0.00	0.00
March	303.92	298.18	98.11	31.73	10.64	0.00	0.00
April	570.20	558.35	97.92	76.40	13.68	0.01	0.00
May	327.50	321.80	98.26	30.25	9.40	2.79	0.87
June	400.18	389.43	97.31	70.01	17.98	11.25	2.89
July	793.62	768.16	96.79	99.97	13.01	18.37	2.39
August	699.14	652.41	93.31	113.48	17.39	134.14	20.56
September	506.77	496.78	98.03	63.93	12.87	3.61	0.73
October	711.48	697.60	98.05	150.13	21.52	3.54	0.51
November	756.74	742.61	98.13	119.69	16.12	0.01	0.00
December	283.43	278.23	98.16	166.50	59.84	0.00	0.00

Table A2: Modelled monthly precipitation, snowfall, erosion, and melt (in mm and %) for the -1 °C scenario. Percentages are relative to total monthly precipitation.

Month	Precipitation (mm)	Snowfall (mm)	Snowfall (%)	Erosion (mm)	Erosion (%)	Melt (mm)	Melt (%)
January	399.02	391.14	98.03	168.44	43.06	0.00	0.00
February	389.98	382.57	98.10	199.06	52.03	0.00	0.00
March	303.92	298.04	98.07	36.78	12.34	0.00	0.00
April	570.20	558.59	97.96	79.93	14.31	0.00	0.00
May	327.50	321.84	98.27	35.79	11.12	1.44	0.45
June	400.18	392.30	98.03	72.82	18.56	6.52	1.66
July	793.62	776.76	97.88	108.62	13.98	10.99	1.42
August	699.14	669.30	95.73	142.32	21.26	15.03	2.25
September	506.77	496.78	98.03	72.87	14.67	1.96	0.40
October	711.48	697.60	98.05	163.14	23.39	1.70	0.24
November	756.74	742.66	98.14	142.52	19.19	0.00	0.00
December	283.43	278.24	98.17	174.01	62.54	0.00	0.00

Table A3: Modelled monthly precipitation, snowfall, erosion, and melt (in mm and %) for the -2 °C scenario. Percentages are relative to total monthly precipitation.

Month	Precipitation (mm)	Snowfall (mm)	Snowfall (%)	Erosion (mm)	Erosion (%)	Melt (mm)	Melt (%)
January	399.02	391.24	98.05	181.46	46.38	0.00	0.00
February	389.98	382.47	98.07	209.66	54.82	0.00	0.00
March	303.92	298.21	98.12	38.87	13.03	0.00	0.00
April	570.20	558.62	97.97	83.65	14.97	0.00	0.00
May	327.50	321.72	98.24	41.09	12.77	0.88	0.27
June	400.18	392.89	98.18	76.11	19.37	3.27	0.83
July	793.62	778.69	98.12	119.22	15.31	3.69	0.47
August	699.14	674.07	96.41	180.83	26.83	10.54	1.56
September	506.77	496.79	98.03	85.53	17.22	1.09	0.22
October	711.48	696.47	97.89	176.95	25.41	0.74	0.11
November	756.74	743.19	98.21	163.99	22.07	0.00	0.00
December	283.43	278.57	98.29	178.02	63.91	0.00	0.00

Table A4: Modelled monthly precipitation, snowfall, erosion, and melt (in mm and %) for the -3 °C scenario. Percentages are relative to total monthly precipitation.

Month	Precipitation (mm)	Snowfall (mm)	Snowfall (%)	Erosion (mm)	Erosion (%)	Melt (mm)	Melt (%)
January	399.02	390.87	97.96	182.87	46.79	0.00	0.00
February	389.98	382.92	98.19	205.93	53.78	0.00	0.00
March	303.92	297.89	98.01	39.84	13.37	0.00	0.00
April	570.20	558.45	97.94	84.86	15.20	0.00	0.00
May	327.50	322.52	98.48	41.29	12.80	0.40	0.12
June	400.18	392.81	98.16	78.42	19.96	2.02	0.51
July	793.62	779.20	98.18	128.57	16.50	1.96	0.25
August	699.14	683.58	97.77	227.48	33.28	8.81	1.29
September	506.77	496.70	98.01	92.53	18.63	0.52	0.10
October	711.48	696.36	97.88	188.06	27.01	0.37	0.05
November	756.74	743.32	98.23	174.37	23.46	0.00	0.00
December	283.43	277.65	97.96	179.89	64.79	0.00	0.00

Table A5: Modelled monthly precipitation, snowfall, erosion, and melt (in mm and %) for the +1 °C scenario. Percentages are relative to total monthly precipitation.

Month	Precipitation (mm)	Snowfall (mm)	Snowfall (%)	Erosion (mm)	Erosion (%)	Melt (mm)	Melt (%)
January	399.02	391.52	98.12	139.60	35.66	0.00	0.00
February	389.98	383.06	98.23	156.05	40.74	0.00	0.00
March	303.92	298.17	98.11	25.50	8.55	0.00	0.00
April	570.20	558.43	97.94	74.75	13.39	0.10	0.02
May	327.50	320.94	98.00	25.32	7.89	3.33	1.04
June	400.18	372.66	93.12	60.43	16.22	45.07	12.09
July	793.62	704.72	88.80	81.76	11.60	204.46	29.01
August	699.14	625.88	89.52	88.45	14.13	468.78	74.90
September	506.77	490.09	96.71	56.03	11.43	6.78	1.38
October	711.48	697.28	98.00	137.27	19.69	5.37	0.77
November	756.74	743.21	98.21	95.89	12.90	0.03	0.00
December	283.43	277.78	98.01	158.07	56.90	0.00	0.00

Table A6: Modelled monthly precipitation, snowfall, erosion, and melt (in mm and %) for the +2 °C scenario. Percentages are relative to total monthly precipitation.

Month	Precipitation (mm)	Snowfall (mm)	Snowfall (%)	Erosion (mm)	Erosion (%)	Melt (mm)	Melt (%)
January	399.02	391.35	98.08	119.75	30.60	0.00	0.00
February	389.98	382.62	98.11	122.57	32.03	0.00	0.00
March	303.92	298.34	98.16	18.57	6.22	0.01	0.00
April	570.20	558.14	97.89	60.88	10.91	0.42	0.08
May	327.50	317.13	96.83	21.61	6.81	4.47	1.41
June	400.18	339.03	84.72	54.70	16.13	226.89	66.92
July	793.62	554.55	69.88	54.89	9.90	720.78	129.98
August	699.14	455.89	65.21	56.74	12.45	800.71	175.64
September	506.77	482.03	95.12	51.29	10.64	23.83	4.94
October	711.48	696.19	97.85	119.81	17.21	7.29	1.05
November	756.74	743.97	98.31	80.70	10.85	0.20	0.03
December	283.43	277.66	97.96	147.60	53.16	0.00	0.00

Table A7: Modelled monthly precipitation, snowfall, erosion, and melt (in mm and %) for the +3 °C scenario. Percentages are relative to total monthly precipitation.

Month	Precipitation (mm)	Snowfall (mm)	Snowfall (%)	Erosion (mm)	Erosion (%)	Melt (mm)	Melt (%)
January	399.02	391.50	98.12	108.29	27.66	0.00	0.00
February	389.98	382.30	98.03	96.11	25.14	0.00	0.00
March	303.92	298.07	98.07	12.46	4.18	0.13	0.04
April	570.20	557.81	97.83	54.04	9.69	1.41	0.25
May	327.50	307.78	93.98	19.55	6.35	4.66	1.51
June	400.18	305.29	76.29	44.60	14.61	567.30	185.82
July	793.62	459.47	57.90	30.70	6.68	1238.56	269.56
August	699.14	286.19	40.93	34.01	11.88	1177.68	411.51
September	506.77	434.08	85.66	45.10	10.39	78.02	17.97
October	711.48	690.84	97.10	107.09	15.50	15.61	2.26
November	756.74	743.42	98.24	70.73	9.51	1.47	0.20
December	283.43	278.60	98.29	143.01	51.33	0.00	0.00

APPENDIX B: Missing wind speed records

Table B1: Monthly percentage of missing 15-minutes wind speed records. The total represents the percentage over the entire dataset.

Month	Missing wind speed records (%)
January	12
February	0
March	0
April	0
May	22
June	22
July	2
August	5
September	0
October	2
November	8
December	11
Total	7

Data availability. The datasets from this study are publicly available at https://doi.org/10.5281/zenodo.15669722 (Carturan, 2025). The data files are stored in CSV format.

Author contribution. TLZ, LC, and ML designed the methodological approach. PG, LC, and GDF carried out the fieldwork. TLZ processed the meteorological data. TLZ ran the model with contributions from ML, NW, and MB. TLZ and LC performed the erosion analysis. TLZ and LC prepared the first draft. All authors contributed to the discussion and the final version of the manuscript.

Competing interests. The contact author has declared that none of the authors has any competing interests.

Acknowledgements. TLZ acknowledges the support and hospitality of the WSL Institute for Snow and Avalanche Research SLF (Davos, Switzerland) for hosting her during her PhD research stay. The authors are grateful to all the students, technicians, and scientists who contributed to the field activities in the period from 2009 to 2016; the alpine guides of the Alpinschule of Solda; the helicopter companies Airway, Air Service Center, and Star Work Sky; and the Hotel Franzenshöhe for logistical support. The authors acknowledge the editor and reviewers for their comments and suggestions.

Financial support. The research was funded by the Italian MIUR Project (PRIN 2010-11), "Response of morphoclimatic system dynamics to global changes and related geomorphological hazards" (the local and national coordinators are Giancarlo Dalla Fontana and Carlo Baroni), and was carried out within the RETURN Extended Partnership and received funding from the European Union NextGenerationEU (National Recovery and Resilience Plan – NRRP, Mission 4, Component 2, Investment 1.3 – D.D. 1243 2/8/2022, PE0000005). The core samples were obtained as part of the Mt Ortles Ice Core Project funded by NSF awards 1060115 and 1461422 with the logistical support of Ripartizione Protezione antincendi e civile of the Autonomous Province of Bolzano in collaboration with the Ripartizione Opere idrauliche e Ripartizione Foreste of the Autonomous Province of Bolzano and the Stelvio National Park. This is Ortles project publication 14 (https://www.ortles.org).

References

Adler, S., Das Klima von Tirol-Südtirol-Belluno: 1981–2010; Vergangenheit-Gegenwart-Zukunft, Zentralanstalt für Meteorologie und Geodynamik; Südtirol Abteilung Brand- und Zivilschutz, Bozen, 102, 2015.

Avanzi, F., Ercolani, G., Gabellani, S., Cremonese, E., Pogliotti, P., Filippa, G., Morra di Cella, U., Ratto, S., Stevenin, H., Cauduro, M., and Juglair, S.: Learning about precipitation lapse rates from snow course data improves water balance modeling. Hydrol. Earth Syst. Sci. 25, 2109–2131. https://doi.org/10.5194/hess-25-2109-2021, 2021.

Ayala, A., Pellicciotti, F., and Shea, J. M.: Modeling 2m air temperatures over mountain glaciers: Exploring the influence of katabatic cooling and external warming, J Geophys Res, 120, 3139–3157, https://doi.org/10.1002/2015JD023137, 2015.

Bartelt, P. and Lehning, M.: A physical SNOWPACK model for the Swiss avalanche warning Part I: numerical model, Cold Reg. Sci. Technol., 35, 123–145, 2002.

Bavay, M., Lehning, M., Jonas, T. and Löwe, H.: Simulations of future snow cover and discharge in Alpine headwater catchments. Hydrol. Process., 23: 95-108. https://doi.org/10.1002/hyp.7195, 2009.

Bavay, M. and Egger, T.: MeteoIO 2.4.2: A preprocessing library for meteorological data, Geosci Model Dev, 7, 3135–3151, https://doi.org/10.5194/gmd-7-3135-2014, 2014.

Beniston, M.: The 2003 heat wave in Europe: A shape of things to come? An analysis based on Swiss climatological data and model simulations, Geophys. Res. Lett., 31, L02202, https://doi.org/10.1029/2003GL018857, 2004.

Bohleber, P.: Alpine Ice Cores as Climate and Environmental Archives. In P. Bohleber, Oxford Research Encyclopedia of Climate Science. Oxford University Press, https://doi.org/10.1093/acrefore/9780190228620.013.743, 2019.

Brunetti, M., Lentini, G., Maugeri, M., Nanni, T., Auer, I., Bohm, R., and Schoner, W.: Climate variability and change in the Greater Alpine Region over the last two centuries based on multi-variable analysis. International Journal of Climatology, 29(15), 2197-2225, https://dx.doi.org/10.1002/joc.1857, 2009.

Capt, M., Bosson, J. B., Fischer, M., Micheletti, N., and Lambiel, C.: Decadal evolution of a very small heavily debris-covered Glacier in an Alpine permafrost environment, Journal of Glaciology, 62, 535–551, https://doi.org/10.1017/jog.2016.56, 2016.

Carrivick, J. L., Berry, K., Geilhausen, M., James, W. H. M., Williams, C., Brown, L. E., Rippin, D. M., and Carver, S. J.: Decadal-Scale Changes of the Ödenwinkelkees, Central Austria, Suggest Increasing Control of Topography and Evolution Towards Steady State, Geografiska Annaler, Series A: Physical Geography, 97, 543–562, https://doi.org/10.1111/geoa.12100, 2015.

Carturan L., Dalla Fontana, G., and Borga, M.: Estimation of winter precipitation in a high-altitude catchment of the Eastern Italian Alps: validation by means of glacier mass balance observations, Geogr. Fis. e Din. Quat., 35, 37-48, https://doi.org/10.4461/GFDQ.2012.35.4, 2012.

Carturan, L., Filippi, R., Seppi, R., Gabrielli, P., Notarnicola, C., Bertoldi, L., Paul, F., Rastner,P., Cazorzi, F., Dinale, R., and Dalla Fontana, G.: Area and volume loss of the glaciers in the Ortles-Cevedale group (Eastern Italian Alps): controls and imbalance of the remaining glaciers, Cryosphere, 7, 1339–1359, https://doi.org/10.5194/tc-7-1339-2013, 2013.

Carturan, L., De Blasi, F., Cazorzi, F., Zoccatelli, D., Bonato, P., Borga, M., and Dalla Fontana, G.: Relevance and scale dependence of hydrological changes in glacierized catchments: insights from historical data series in the eastern Italian Alps, Water, 11(1), 89, https://doi.org/10.3390/w11010089, 2019.

Carturan, L., De Blasi, F., Dinale, R., Dragà, G., Gabrielli, P., Mair, V., Seppi, R., Tonidandel, D., Zanoner, T., Zendrini, T. L., and Dalla Fontana, G.: Modern air, englacial and permafrost temperatures at high altitude on Mt Ortles (3905 m a.s.l.), in the eastern European Alps, Earth Syst. Sci. Data, 15, 4661–4688, https://doi.org/10.5194/essd-15-4661-2023, 2023.

Carturan L., Ihle A. C., .Cazorzi F., Zendrini T.L., De Blasi F., Dalla Fontana G., Dreossi G., Festi D., Mark B., Oeggl K.D., Seppi R., Stenni B., Gabrielli P.: Reconstruction of mass balance and firn stratigraphy during the 1996–2011 warm period at high-altitude on Mt. Ortles, Eastern Alps: a comparison of modelled and ice core results. The Cryosphere, 19, 3443–3458, 2025. https://doi.org/10.5194/tc-19-3443-2025. 2025.

Clark, M. P., Hendrikx, J., Slater, A. G., Kavetski, D., Anderson, B., Cullen, N. J., Woods, R., Zammit, C., and Schmidt, J.: Representing spatial variability of snow water equivalent in hydrologic and land-surface models: A review, Water Resour. Res., 47, W07539, https://doi.org/10.1029/2011WR010745, 2011.

Cremona, A., Huss, M., Landmann, J. M., Schwaizer, G., Paul, F., Farinotti, D.: Constraining sub-seasonal glacier mass balance in the Swiss Alps using Sentinel-2-derived snow-cover observations. J. Glaciol., ;71:e25. doi:10.1017/jog.2025.1, 2025.

De Blasi F.: Scale dependence of hydrological effects from different climatic conditions on glacierized catchments, PhD thesis, University of Padova, 2018.

Dumont, M., Monteiro, D., Filhol, S., Gascoin, S., Marty, C., Hagenmuller, P., Morin, S., Choler, P., and Thuiller, W.: The European Alps in a changing climate: physical trends and impacts, C. R. Géosci., 357, 25–42, https://doi.org/10.5802/crgeos.288, 2025.

Evans, M. N., Tolwinski-Ward, S. E., Thompson, D. M., and Anchukaitis, K. J.: Applications of proxy system modeling in high resolution paleoclimatology, Quaternary Sci. Rev., 76, 16-28, https://doi.org/10.1016/j.quascirev.2013.05.024, 2013.

Fierz, C., Armstrong, R.L., Durand, Y., Etchevers, P., Greene, E., McClung, D.M., Nishimura, K., Satyawali, P.K. and Sokratov, S.A.: The International Classification for Seasonal Snow on the Ground. IHP-VII Technical Documents in Hydrology N°83, IACS Contribution N°1, UNESCO-IHP, Paris, 2009.

Gabrielli, P., Carturan, L., Gabrieli, J., Dinale, R., Krainer, K., Hausmann, H., Davis, M., Zagorodnov, V., Seppi, R., Barbante, C., Fontana, G. D., and Thompson, L. G.: Atmospheric warming threatens the untapped glacial archive of Ortles mountain, South Tyrol, J. Glaciol,, 56, 843–853, https://doi.org/10.3189/002214310794457263, 2010.

Gabrielli, P., Barbante, C., Carturan, L., Cozzi, G., Dalla Fontana, G., Dinale, R., Draga, G., 562 Gabrieli, J., Kehrwald, N., Mair, V., Mikhalenko, V. N., Piffer, G., Rinaldi, M., Seppi, R., Spolaor, A., Thompson, L. G., and Tonidandel, D.: Discovery of cold ice in a new drilling site in the Eastern European Alps, Geogr. Fis. Dinam. Quat., 35, 101–105, doi:10.4461/GFDQ.2012.35.10, 2012.

Gabrielli, P., Barbante, C., Bertagna, G., Bertó, M., Binder, D., Carton, A., Carturan, L., Cazorzi, F., Cozzi, G., Dalla Fontana, G., Davis, M., De Blasi, F., Dinale, R., Dragà, G., Dreossi, G., Festi, D., Frezzotti, M., Gabrieli, J., Galos, S. P., Ginot, P., Heidenwolf, P., Jenk, T. M., Kehrwald, N., Kenny, D., Magand, O., Mair, V., Mikhalenko, V., Lin, P. N., Oeggl, K., Piffer, G., Rinaldi, M., Schotterer, U., Schwikowski, M., Seppi, R., Spolaor, A., Stenni, B., Tonidandel, D., Uglietti, C., Zagorodnov, V., Zanoner, T., and Zennaro, P.: Age of the Mt. Ortles ice cores, the Tyrolean Iceman and glaciation of the highest summit of South Tyrol since the Northern Hemisphere Climatic Optimum, The Cryosphere, 10, 2779–2797, doi:10.5194/tc-10-2779-2016, 2016.

Gabrielli, P., Jenk, T. M., Bertó, M., Dreossi, G., Festi, D., Kofler, W., Winstrup, M., Oeggl, K., Schwikowski, M., Stenni, B., and Barbante, C.: A multimillennial Alpine ice core chronology synchronized with an accurately dated Arctic Pb record, EGUsphere [preprint], https://doi.org/10.5194/egusphere-2025-2174, 2025.

Gobiet, A., Kotlarski, S., Beniston, M., Heinrich, G., Rajczak, J., and Stoffel, M.: 21st century climate change in the European Alps—A review. Science of the total environment, 493, 1138-1151, https://doi.org/10.1016/j.scitotenv.2013.07.050, 2014.

Haeberli, W., and Alean, J.: Temperature and accumulation of high altitude firn in the Alps, Ann. Glaciol., 6, 161–163, https://doi.org/10.3189/1985AoG6-1-161-163, 1985.

He, S., and Ohara, N.: A new formula for estimating the threshold wind speed for snow movement, J. Adv. Model. Earth. Sy., 9, 2514–2525. https://doi.org/10.1002/2017MS000982, 2017.

Hock, R. and Huss, M.: Glaciers and climate change, 157–176 pp., https://doi.org/10.1016/B978-0-12-821575-3.00009-8, 2021.

Hock, R., Hutchings, J. K., and Lehning, M.: Grand challenges in cryospheric sciences: Toward better predictability of glaciers, snow and sea ice, Front. Earth Sci., 5, 64, https://doi.org/10.3389/feart.2017.00064, 2017.

Houze, R. A.: Orographic effects on precipitating clouds. Reviews of Geophysics, 50(1), https://doi.org/10.1029/2011RG000365, 2012.

Humlum, O-: Glacier behaviour and the influence of upper-air conditions during the Little Ice Age in Disko, central West Greenland. Geografisk Tidsskrift-Danish Journal of Geography, 87(1), 1–12. https://doi.org/10.1080/00167223.1987.10649234, 1987.

Huss, M., Bauder, A., Funk, M., and Hock, R.: Determination of the seasonal mass balance of four Alpine glaciers since 1865, J. Geophys. Res., 113, F01015, doi:10.1029/2007JF000803, 2008.

IPCC: Climate Change 2022: Impacts, Adaptation, and Vulnerability, Contribution of Working Group II to the Sixth Assessment Report of the Intergovernmental Panel on Climate Change, Cambridge University Press, Cambridge, UK and New York, NY, USA, 3056 pp., doi:10.1017/9781009325844, 2022.

Jackson, P. S. and Hunt, J. C. R.: Turbulent wind flow over a low hill. Quarterly Journal of the Royal Meteorological Society, 101(430), 929-955, https://doi.org/10.1002/qj.49710143015, 1975.

Jacquemart, M., Weber, S., Chiarle, M., Chmiel, M., Cicoira, A., Corona, C., Eckert, N., Gaume, J., Giacona, F., Hirschberg, J., Kaitna, R., Magnin, F., Mayer, S., Moos, C., van Herwijnen, A., and Stoffel, M.: Detecting the impact of climate change on alpine mass movements in observational records from the European Alps, Earth-Sci Rev, 258, 104886, https://doi.org/10.1016/j.earscirev.2024.104886, 2024.

Johnson, E. and Rupper, S.: An Examination of Physical Processes That Trigger the Albedo- Feedback on Glacier Surfaces and Implications for Regional Glacier Mass Balance Across High Mountain Asia, Front Earth Sci (Lausanne), 8, https://doi.org/10.3389/feart.2020.00129, 2020.

Kochendorfer, J., Rasmussen, R., Wolff, M., Baker, B., Hall, M. E., Meyers, T., Landolt, S., Jachcik, A., Isaksen, K., Brækkan, R., and Leeper, R.: The quantification and correction of wind-induced precipitation measurement errors, Hydrol. Earth Syst. Sci., 21, 1973–1989, https://doi.org/10.5194/hess-21-1973-2017, 2017.

Konrad, H., Bohleber, P., Wagenbach, D., Vincent, C., and Eisen, O.: Determining the age distribution of Colle Gnifetti, Monte Rosa, Alps, by combining ice cores, ground-penetrating radar and a simple flow model, J. Glaciol., 59, 179–189, https://doi.org/10.3189/2013JoG12J072, 2013.

Kotlarski, S., Gobiet, A., Morin, S., Olefs, M., Rajczak, J., and Samacoïts, R.: 21st Century alpine climate change. Climate Dynamics, 60(1), 65-86, https://doi.org/10.1007/s00382-022-06303-3, 2023.

Lehning, M., Doorschot, J., and Bartelt, P.: A snowdrift index based on SNOWPACK model calculations, Ann. Glaciol., 31, 382–386, https://doi.org/10.3189/172756400781819770, 2000.

Lehning, M., Bartelt, P., Brown, B., and Fierz, C.: A physical SNOWPACK model for the Swiss avalanche warning: Part III: meteorological forcing, thin layer formation and evaluation, Cold Reg Sci Technol, 35, 169–184, https://doi.org/10.1016/S0165-232X(02)00072-1, 2002b.

Lehning, M., Bartelt, P., Brown, B., Fierz, C., and Satyawali, P.: A physical SNOWPACK model for the Swiss avalanche warning: Part II. Snow microstructure, Cold Reg Sci Technol, 35, 147– 167, https://doi.org/10.1016/S0165-232X(02)00073-3, 2002a.

Lehning, M., and Fierz, C.: Assessment of snow transport in avalanche terrain, Cold Reg. Sci. Technol., 51, 240–252, https://doi.org/10.1016/j.coldregions.2007.05.012, 2008.

Lehning, M., Löwe, H., Ryser, M., and Raderschall, N.: Inhomogeneous precipitation distribution and snow transport in steep terrain, Water Resour. Res., 44, W07404, https://doi.org/10.1029/2007WR006545, 2008.

Li, L., and Pomeroy, J. W.: Estimates of threshold wind speeds for snow transport using meteorological data, J. Appl. Meteorol. Climatol., 36, 205–213, https://doi.org/10.1175/1520-0450(1997)036<0205:EOTWSF>2.0.CO;2, 1997b.

Li, L., and Pomeroy, J. W.: Probability of occurrence of blowing snow, J. Geophys. Res.-Atmos., 102, 21955–21964, https://doi.org/10.1029/97JD01522, 1997a.

Meirold-Mautner, I. and Lehning, M.: Measurements and model calculations of the solar shortwave fluxes in snow on Summit, Greenland, Ann Glaciol, 38, 279–284, https://doi.org/10.3189/172756404781814753, 2004.

Mott, R., Schirmer, M., Bavay, M., Grünewald, T., and Lehning, M.: Understanding snow-transport processes shaping the mountain snow cover, The Cryosphere, 4, 545–559, https://doi.org/10.5194/tc-4-545-2010, 2010.

Mott, R., Vionnet, V., and Grünewald, T.: The seasonal snow cover dynamics: review on wind-driven snow transport and sublimation, Front. Earth Sci., 6, 197, https://doi.org/10.3389/feart.2018.00197, 2018.

Obleitner, F. and Lehning, M.: Measurement and simulation of snow and superimposed ice at the Kongsvegen glacier, Svalbard (Spitzbergen), Journal of Geophysical Research: Atmospheres, 109, https://doi.org/10.1029/2003jd003945, 2004.

Owen, P. R.: Saltation of uniform grains in air, J. Fluid Mech., 20, 225–242, 1964.

Panofsky, H.A. , Zhao Ming: Characteristics of wind profiles over complex terrain, Journal of Wind Engineering and Industrial Aerodynamics, Volume 15, Issues 1–3, Pages 177-183, ISSN 0167-6105, https://doi.org/10.1016/0167-6105(83)90188-5, 1983.

Pellegrini, C. C., and Bodstein, G. C. R.: The height of maximum speed-up in the atmospheric boundary layer flow over low hills. Journal of the Brazilian Society of Mechanical Sciences and Engineering, 26(3), 249-259, https://doi.org/10.1590/S1678-58782004000300001, 2004.

Pepin, N., Apple, M., Knowles, J., Terzago, S., Arnone, E., Hänchen, L., Napoli, A., Potter, E., Steiner, J., Williamson, S. N., Ahrens, B., Dhar, T., Dimri, A. P., Palazzi, E., Rameshan, A., Salzmann, N., Shahgedanova, M., de Deus Vidal, J., and Zardi, D.: Elevation-dependent climate change in mountain environments, Nature Reviews Earth & Environment 2025 6:12, 6, 772–788, https://doi.org/10.1038/s43017-025-00740-4, 2025.Pomeroy, J. W., and Gray, D. M.: Saltation of snow, Water Resour. Res., 26, 1583–1594, https://doi.org/10.1029/WR026i007p01583, 1990.

Raderschall, N., Lehning, M., and Schär, C.: Fine-scale modeling of the boundary layer wind field over steep topography. Water Resources Research, 44(9), https://doi.org/10.1029/2007WR006544, 2008.

Rasmus, S., Räisänen, J., and Lehning, M.: Estimating snow conditions in Finland in the late 21st century using the SNOWPACK model with regional climate scenario data as input, Ann Glaciol, 38, 238–244, https://doi.org/10.3189/172756404781814843, 2004.

Rasmussen, R., Baker, B., Kochendorfer, J., Meyers, T., Landolt, S., Fischer, A. P., Black, J., Thériault, J. M., Kucera, P., Gochis, D., Smith, C., Nitu, R., Hall, M., Ikeda, K., & Gutmann, E.: How Well Are We Measuring Snow: The NOAA/FAA/NCAR Winter Precipitation Test Bed. Bulletin of the American Meteorological Society, 93(6), 811-829. https://doi.org/10.1175/BAMS-D-11-00052.1, 2012.

Roe, G. H.: Orographic precipitation. Annu. Rev. Earth Planet. Sci., 33(1), 645-671, https://doi.org/10.1146/annurev.earth.33.092203.122541, 2005.

Schäfer, M., Möller, M., Zwinger, T., and Moore, J. C.: Dynamic modelling of future glacier changes: mass-balance/elevation feedback in projections for the Vestfonna Ice Cap, Nordaustlandet, Svalbard, J. Glaciol., 61(230), 1121–1136, https://doi.org/10.3189/2015JoG14J184, 2015.

Schmidt, R. A.: Threshold wind-speeds and elastic impact in snow transport, J. Glaciol., 26, 453–467, https://doi.org/10.3189/S0022143000010972, 1980.

Schmucki, E., Marty, C., Fierz, C., and Lehning, M.: Simulations of 21st century snow response to climate change in Switzerland from a set of RCMs. International journal of climatology, 35(11), https://doi.org/10.1002/joc.4205, 2015.

Schuler, T. V., Hock, R., Jackson, M., Elvehøy, H., Braun, M., Brown, I., and Hagen, J.-O.: Distributed mass-balance and climate sensitivity modelling of Engabreen, Ann. Glaciol., 42, 395–401. doi:10.3189/172756405781812998, 2005.

Shaw, T. E., Buri, P., McCarthy, M., Miles, E. S., Ayala, Á., and Pellicciotti, F.: The Decaying Near-Surface Boundary Layer of a Retreating Alpine Glacier, Geophys Res Lett, 50, https://doi.org/10.1029/2023gl103043, 2023.

Shaw, T. E., Miles, E. S., McCarthy, M., Buri, P., Guyennon, N., Salerno, F., Carturan, L., Brock, B., and Pellicciotti, F.: Mountain glaciers recouple to atmospheric warming over the twenty-first century, Nat. Clim. Chang., 15, 1212–1218, https://doi.org/10.1038/s41558-025-02449-0, 2025.

Stiperski, I., & Rotach, M.W.:On the Measurement of Turbulence over Complex Mountainous Terrain, Bound.-Lay. Meteorol, 159, 97–121. https://doi.org/10.1007/s10546-015-0103-z , 2016.

Taylor, P. A., Mason, P. J., and Bradley, E. F.: Boundary-layer flow over low hills. Boundary-layer meteorology, 39(1), 107-132, https://doi.org/10.1007/BF00121870, 1987.

Wever, N., Keenan, E., Amory, C., Lehning, M., Sigmund, A., Huwald, H., and Lenaerts, J. T. M.: Observations and simulations of new snow density in the drifting snow-dominated environment of Antarctica, J. Glaciol., 69, 823–840, https://doi.org/10.1017/jog.2022.102, 2023.

Zemp, M., Thibert, E., Huss, M., Stumm, D., Rolstad Denby, C., Nuth, C., Nussbaumer, S. U., Moholdt, G., Mercer, A., Mayer, C., Joerg, P. C., Jansson, P., Hynek, B., Fischer, A., Escher-Vetter, H., Elvehøy, H., and Andreassen, L. M.: Reanalysing glacier mass balance measurement series, The Cryosphere, 7, 1227–1245, https://doi.org/10.5194/tc-7-1227-2013, 2013.

Zhao, F., Long, D., Li, X., Huang, Q., and Han, P.: Rapid glacier mass loss in the Southeastern Tibetan Plateau since the year 2000 from satellite observations, Remote Sens Environ, 270, 112853, https://doi.org/10.1016/J.RSE.2021.112853, 2022.